C-Jun N-terminal Kinase Promotes Stress Granule Assembly and Neurodegeneration in C9orf72-mediated ALS and FTD

Sahana TG[1], Katherine Johnson Chase[1], Feilin Liu[1], Thomas E. Lloyd[2], Wilfried Rossoll[1,3], and Ke Zhang[1,3]

[1] Department of Neuroscience, Mayo Clinic, Jacksonville, FL 32224, USA

[2] Department of Neurology, Johns Hopkins School of Medicine, MD 21205, USA

[3] Neuroscience Graduate Program, Mayo Clinic Graduate School of Biomedical Sciences, Jacksonville, FL 32224, USA

Send correspondence to:

Ke Zhang, Department of Neuroscience, Mayo Clinic, 4500 San Pablo Rd S, Jacksonville, FL 32224, USA. Email: zhang.ke@mayo.edu

Abstract

Stress granules (SGs), RNA/protein condensates assembled in cells under stress, are believed to play a critical role in the pathogenesis of amyotrophic lateral sclerosis (ALS) and frontotemporal dementia (FTD). However, how SG assembly is regulated and related to pathomechanism is incompletely understood. Here, we show that ER stress activates JNK via IRE1 in fly and cellular models of C9orf72-mediated ALS/FTD (c9ALS/FTD), the most common genetic form of ALS/FTD. Furthermore, activated JNK promotes SG assembly induced by poly(GR) and poly(PR), two toxic proteins implicated in c9ALS/FTD, by promoting the transcription of G3BP1, a key SG protein. Consistent with these findings, JNK or IRE1 inhibition reduced SG formation, G3BP1 mRNA and protein levels, and neurotoxicity in cells overexpressing poly(GR) and poly(PR) or neurons derived from c9ALS/FTD patient induced pluripotent stem cells (iPSCs). Our findings connect ER stress, JNK, and SG assembly in a unified pathway contributing to c9ALS/FTD neurodegeneration.

Introduction

A GGGGCC (G_4C_2) hexanucleotide repeat expansion in chromosome 9, open reading frame 72 (*C9ORF72*) is the most common genetic cause of amyotrophic lateral sclerosis (ALS) and frontotemporal dementia (FTD) (DeJesus-Hernandez et al., 2011; Renton et al., 2011). This repeat expansion can cause cytotoxicity via multiple mechanisms, one of which suggests that it undergoes repeat-associated, non-ATG translation to produce five different species of dipeptide repeat proteins (DPRs), namely poly(glycine-arginine, GR), poly(glycine-alanine, GA), poly(glycine-proline, GP), poly(proline-alanine, PA), and poly(proline-arginine, PR)(Ash et al., 2013; Donnelly et al., 2013; Gendron et al., 2013; Ling, Polymenidou, & Cleveland, 2013; Mori, Arzberger, et al.,

2013; Mori, Weng, et al., 2013; Zu et al., 2013). Among these DPRs, the arginine-rich DPRs (R-DPRs) i.e., poly(GR), and poly(PR), are especially toxic (Kwon et al., 2014; K. H. Lee et al., 2016; Lin et al., 2016; Mizielinska et al., 2014; Sakae et al., 2018; K. Zhang et al., 2018; Y. J. Zhang et al., 2018; Zhang et al., 2019).

Stress granules (SGs) are cytoplasmic RNA/protein condensates assembled in cells under stress (Protter & Parker, 2016). Upon stress, polysomes disassemble, and mRNAs are embedded by a variety of RNA-binding proteins, whose condensation mediates SG assembly (Guillen-Boixet et al., 2020; Sanders et al., 2020; P. Yang et al., 2020). Under normal conditions, SGs are dynamic and disassemble when stress is removed (Lin, Protter, Rosen, & Parker, 2015; Protter & Parker, 2016). However, aberrant SG formation can trigger aggregation of SG proteins, such as TDP-43 and FUS (A.N. Coyne et al., 2015; Daigle et al., 2013). Since the aggregation of these proteins is a pathological hallmark of ALS and FTD, including c9ALS/FTD, SGs are believed to play a critical role in ALS/FTD pathogenesis (Anderson & Kedersha, 2008; Kedersha, Tisdale, Hickman, & Anderson, 2008; Li, King, Shorter, & Gitler, 2013). Consistent with this notion, R-DPRs interact with many SG proteins, and their overexpression causes the formation of aberrant, poorly dynamic SGs in cells without additional stress (Boeynaems et al., 2017; K. H. Lee et al., 2016; K. Zhang et al., 2018). In addition, chemically synthesized R-DPRs can undergo liquid-liquid phase separation (LLPS), recruit SG proteins, and cause SG protein precipitation in cellular lysates (Boeynaems et al., 2017). Also, poly(GR) can localize to SGs, promote the aggregation of recombinant TDP-43 *in vitro*, and co-aggregate with TDP-43 and the SG protein eIF3η in c9ALS/FTD patient postmortem tissue (Cook et al., 2020). In agreement with these data, we previously found that inhibiting SG assembly by genetic or pharmacological approaches suppresses R-DPR-induced cytotoxicity or neurodegeneration in cellular or animal models (K. Zhang et al., 2018). Together,

these findings suggest that R-DPRs cause neurodegeneration by promoting aberrant SG formation. However, how this process is regulated is unclear.

In a *Drosophila* RNAi screen, we previously identified that loss of *bsk*, the fly homolog of c-Jun N-terminal kinase (JNK), suppresses neurodegeneration in a fly model of c9ALS/FTD (K. Zhang et al., 2015). Here, we show that JNK is activated in fly and cellular models of c9ALS/FTD via ER stress response protein IRE1 and activated JNK promotes R-DPR-induced SG formation by promoting the transcription of G3BP1, a key protein involved in SG assembly (Deniz, 2020; Guillen-Boixet et al., 2020; P. Yang et al., 2020). Inhibiting ER stress responses or JNK activity suppresses R-DPR-induced SG formation, G3BP1 mRNA and protein levels, and cytotoxicity in cells expressing R-DPRs or c9ALS/FTD patient iPSC-derived neurons (iPSNs). Our findings identified a molecular mechanism by which the ER stress/IRE1/JNK axis promotes long-term-stress-induced SG formation and suggested a unified, druggable pathway contributing to c9ALS/FTD pathogenesis.

Results

Loss of *bsk/JNK* suppresses neurodegeneration caused by G_4C_2 repeats in *Drosophila*

Expression of 30 G_4C_2 repeats [$(G_4C_2)_{30}$] in fly eyes using GMR-GAL4 causes neurodegeneration, as indicated by defects in the external eye morphology that worsen with age (Xu et al., 2013; K. Zhang et al., 2015). Using this fly model, our previously published RNAi screen identified *bsk* RNAi to potently suppress $(G_4C_2)_{30}$-mediated eye degeneration (K. Zhang et al., 2015), which we verified (**Fig. 1a**). Furthermore, we show that $(G_4C_2)_{30}$ expression in motor neurons using vGlut-GAL4 causes paralysis in pharate flies, as indicated by their inability to eclose (Cunningham et al., 2020). Here, we show that *bsk* RNAi suppresses this phenotype (**Fig. 1b**). Thus, loss of *bsk* suppresses $(G_4C_2)_{30}$-mediated toxicity in fly eyes and motor neurons.

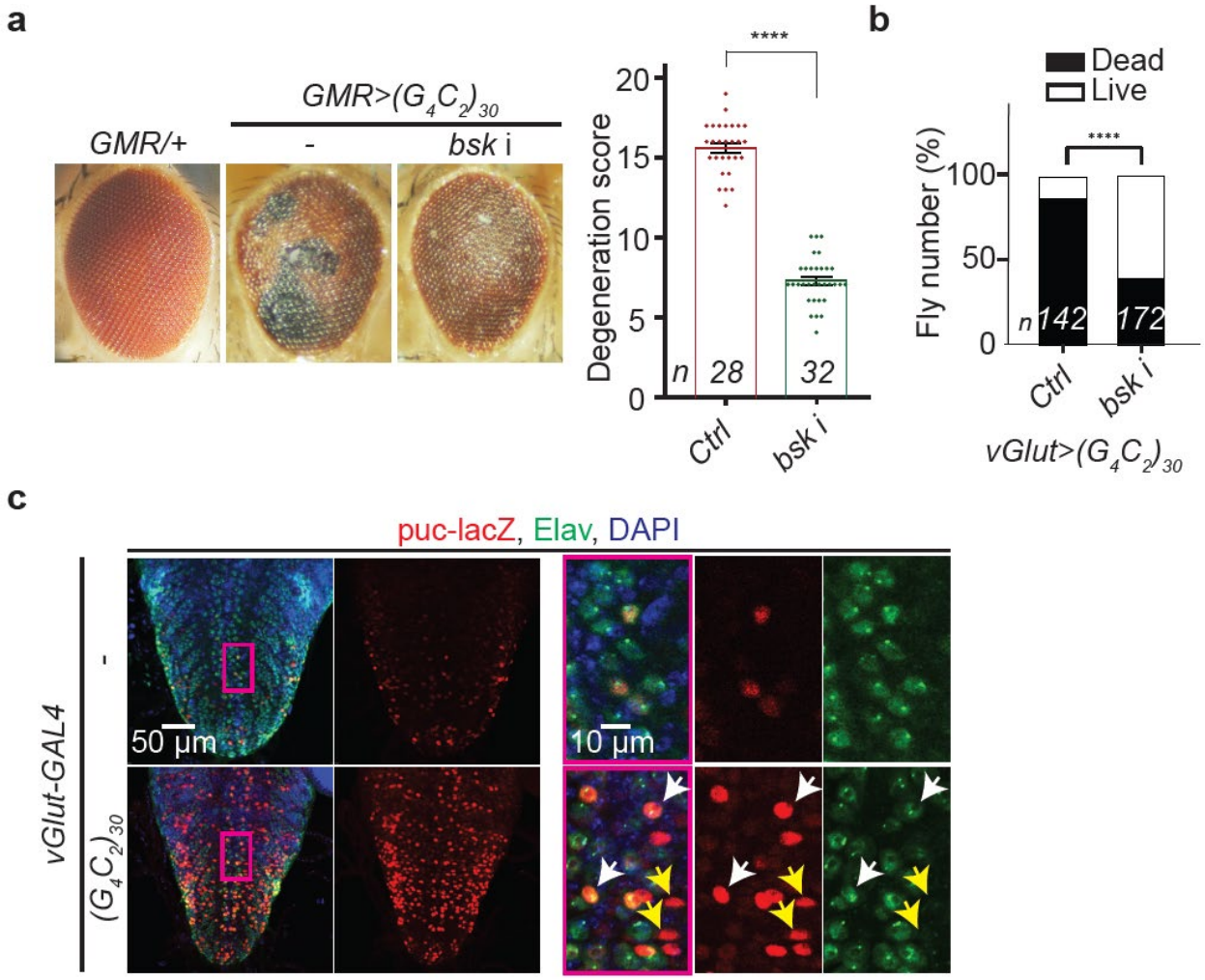

Figure 1: JNK/bsk is activated in a fly model of c9ALS/FTD. (a) Fly eyes expressing $(G_4C_2)_{30}$ using GMR-GAL4, without or with *bsk* RNAi (*bsk* i). Scored using a previously published method (G.P. Ritson et al., 2010). Mean ± s.e.m. Student's t-test; ****: $p<0.0001$ (b) Percent of eclosed adult flies expressing $(G_4C_2)_{30}$ in motor neurons using vGlut-GAL4, without (control, Ctrl) or with *bsk* i. $\chi 2$-test; ****: $p<0.0001$ (c) Fly ventral nerve cord motor neurons expressing puc-lacZ without or with co-expressing $(G_4C_2)_{30}$, stained with lacZ (red), Elav (a neuronal marker, green), and DAPI (blue).

Next, we tested whether Bsk is hyperactive in neurons expressing G_4C_2 repeats. Bsk/JNK belongs to the mitogen-activated protein kinase (MAPK) family, which is activated by JNK kinases (Kim & Choi, 2010; Sahana & Zhang, 2021). Upon activation, Bsk/JNK activates the transcription of downstream genes, including its inhibitor, JNK phosphatase (fly homolog: *puckered*, or *puc*). Thus, the level of Puc/JNK phosphate can be used to indicate Bsk/JNK activity. Indeed, a LacZ reporter under the control of the *puc* promoter (puc-LacZ) is widely used as a

reporter of Bsk/JNK activity in flies (Martin-Blanco et al., 1998; Ring & Arias, 1993). Using this reporter, we show that the LacZ level is strongly upregulated in motor neurons expressing $(G_4C_2)_{30}$, compared to the control (**Fig. 1c**), suggesting that expression of G_4C_2 repeats causes JNK activation.

Expression of G_4C_2 repeats causes ER stress in *Drosophila*

Previous studies showed that JNK can be activated by ER stress. Upon ER stress, inositol requiring enzyme 1 (IRE1), a protein with both kinase and endonuclease activities, is activated, which recruits the tumor necrosis factor receptor-associated factor 2 (TRAF2). The IRE1/TRAF2 complex phosphorylates and activates apoptosis signal-regulating kinase (ASK-1), a MAP kinase kinase kinase (MAP3K), which activates its downstream target JNK (Urano et al., 2000). Furthermore, previous studies have implicated ER stress in c9ALS/FTD iPSNs (Dafinca et al., 2016; Haeusler et al., 2014). Here, we show that RNAi against IRE1, TRAF2, or ASK-1 suppresses eye degeneration in flies expressing $(G_4C_2)_{30}$, suggesting that these proteins contribute to G_4C_2-repeat-mediated neurotoxicity (**Fig. 2a**).

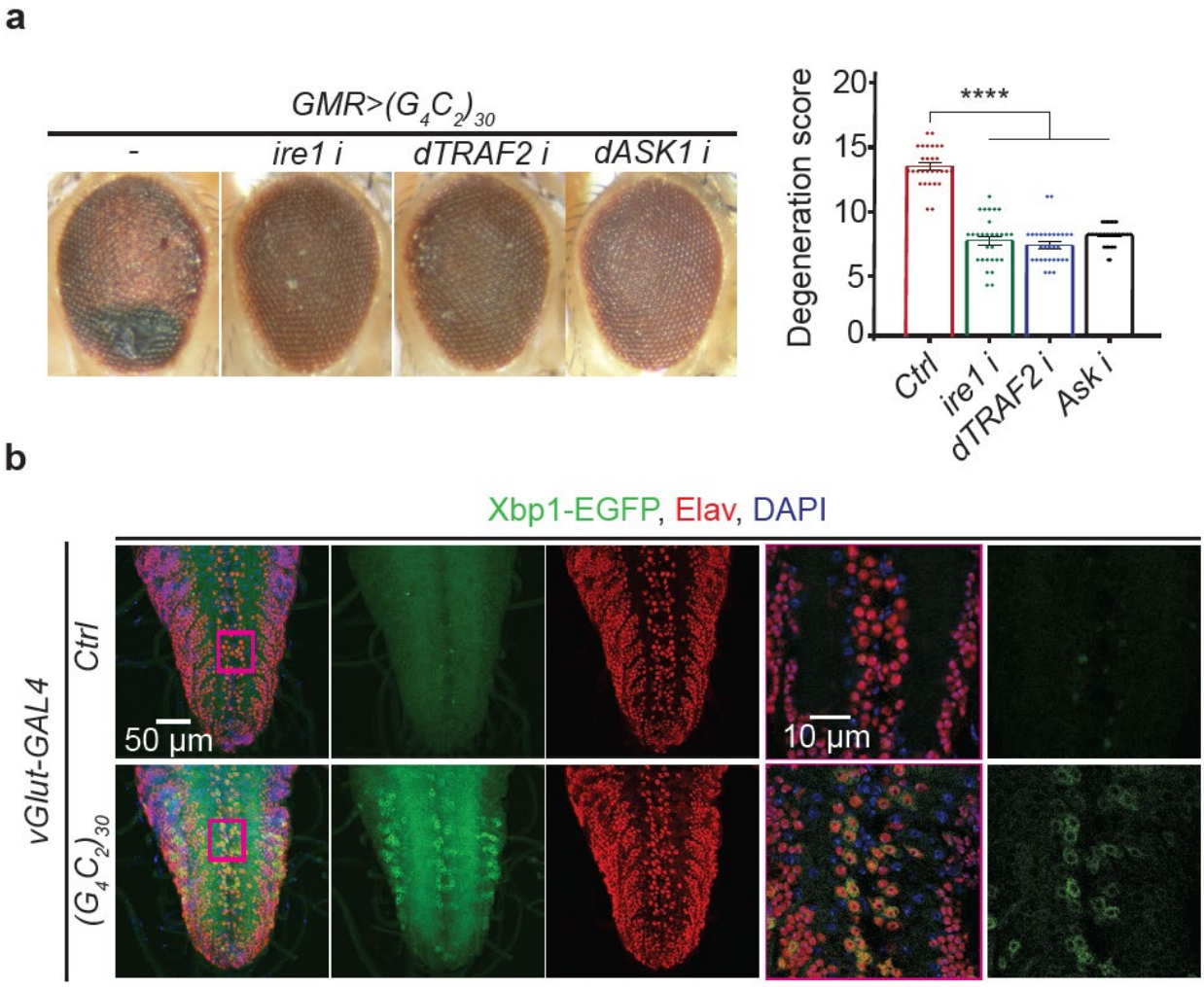

Figure 2: ER stress contributes to neurodegeneration in a fly model of c9ALS/FTD. (a) Fly eyes expressing $(G_4C_2)_{30}$ without or with RNAi against ire1, dASK1 and dTRAF2. Mean ± s.e.m. One-way ANOVA; ****: $p<0.0001$. (b) Fly VNC motor neurons expressing Xbp1-GFP without or with $(G_4C_2)_{30}$, stained with Elav (a neuronal marker, red) and DAPI (blue).

Next, we investigated the IRE1 activity in fly neurons. Upon IRE1 activation, its endonuclease activity causes the alternative splicing of X-box-binding protein 1 (XBP1) mRNA. In fly studies, a widely used IRE1 reporter is an XBP1-GFP system, in which GFP is expressed only when XBP1 is alternatively spliced due to IRE1 activation (Sone, Zeng, Larese, & Ryoo, 2013). Using this system, we show that GFP is strongly upregulated in motor neurons expressing $(G_4C_2)_{30}$, compared to the control (**Fig. 2b**), suggesting that expression of G_4C_2 repeats causes IRE1 activation.

Together, our data suggest that G_4C_2 repeats cause ER stress, further leading to toxicity in *Drosophila*.

R-DPRs cause JNK activation and ER stress in U-2 OS cells

Among five DPR species, the R-DPRs, i.e., poly(GR) and poly(PR), are highly toxic and cause eye degeneration and cytotoxicity in *Drosophila* and cultured cells (Mizielinska et al., 2014). Thus, we investigated their roles in JNK activation and ER stress. First, we show that *bsk* RNAi suppresses eye degeneration caused by 36 repeats of poly(GR) or poly(PR) (**Supplementary Fig. 1**), suggesting that JNK contributes to poly(GR) and poly(PR)-mediated toxicity. Next, we switched to U-2 osteosarcoma (OS) cells, which are widely used to study cellular stress responses and R-DPR toxicity for their human relevance and ease to dissect cellular mechanisms (Boeynaems et al., 2017; Kwon et al., 2014; Ohn, Kedersha, Hickman, Tisdale, & Anderson, 2008; P. Yang et al., 2020).

Using an MTT cell survival assay, we show that transiently expressing mCherry-tagged, 100 repeats of poly(GR) or poly(PR) [$(GR)_{100}$- or $(PR)_{100}$-mCherry] for 48 hours impairs U-2 OS cell survival, compared to the mCherry control, which is partially suppressed by a 24-hour co-treatment of a pan-JNK inhibitor, SP600125 (**Fig. 3a**). These data suggest that inhibiting JNK activity suppresses R-DPR-mediated cytotoxicity, consistent with our fly data (**Supplementary Fig. 1**). Furthermore, both our immunofluorescent staining and Western blots show that $(GR)_{100}$- and $(PR)_{100}$-mCherry increase the levels of phosphorylated JNK (pJNK), the activated JNK form, compared to the mCherry control (**Fig. 3b and c**), suggesting that R-DPRs activate JNK in U-2 OS cells.

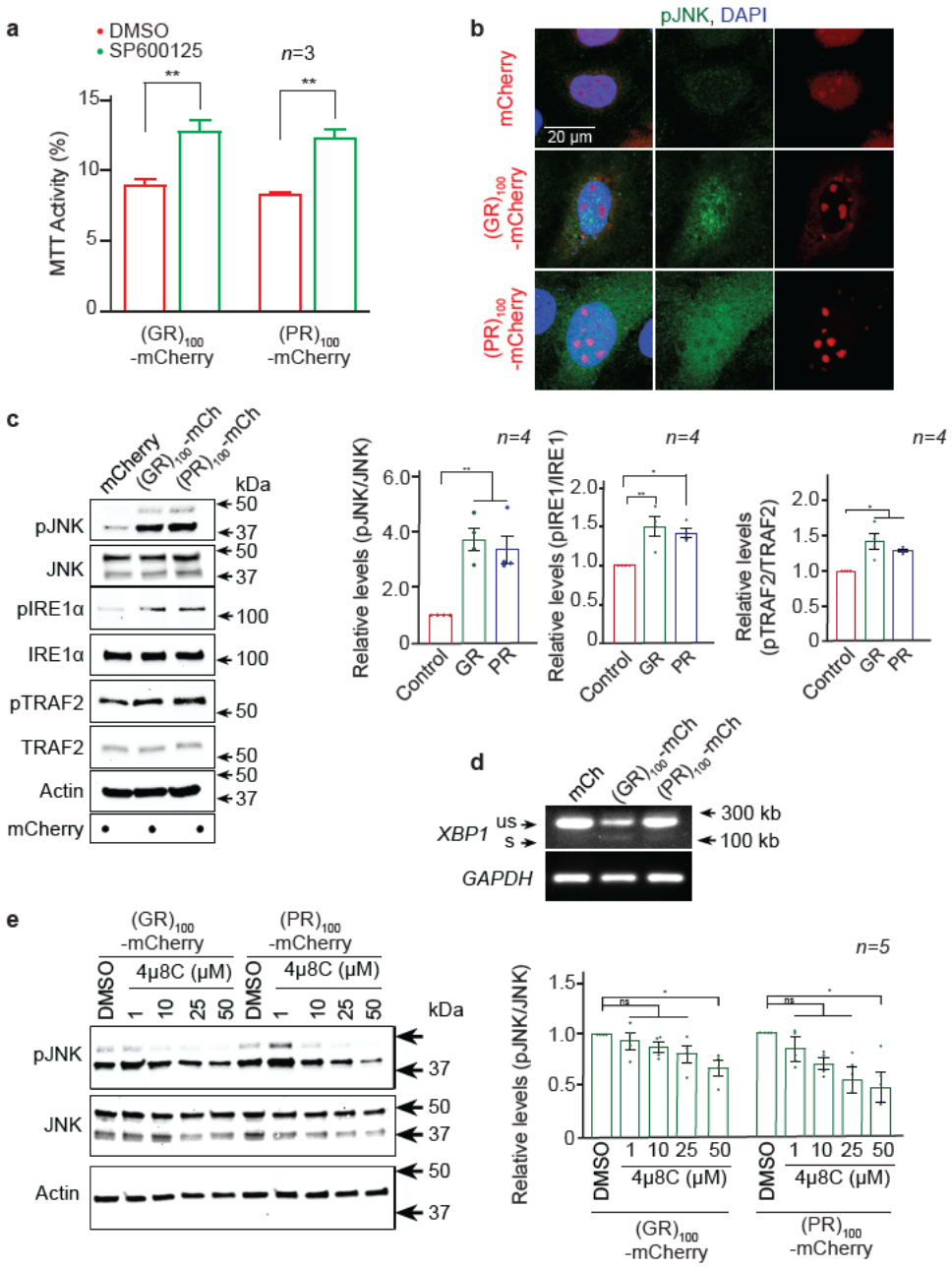

Figure 3: ER stress and JNK is activated in U-2 OS cells expressing R-DPRs. (a) MTT assays of U-2 OS cells expressing (GR/PR)$_{100}$-mCherry, treated with DMSO or 50 μM of SP600125 for 24 h. MTT activity of U-2 OS cells expressing mCherry is taken as 100%. Mean ± s.e.m. Student's t-tests; **, p<0.01. (b) U-2 OS cells expressing mCherry or (GR/PR)$_{100}$-mCherry (red) stained with pJNK (green) and DAPI (blue). (c) Western or dot (for mCherry only) blots for lysates from U-2 OS cell expressing mCherry or (GR/PR)$_{100}$-mCherry. Mean ± s.e.m. One-way ANOVA; **, p<0.01; *, p<0.05. (d) DNA gels showing spliced variants of XBP1 (us: unspliced and s: spliced) from cDNA of U-2 OS cell expressing mCherry or (GR/PR)$_{100}$-mCherry. (e) Western blots for lysates from U-2 OS cell expressing mCherry or (GR/PR)$_{100}$-mCherry co-treated with DMSO or 4μ8C for 6 h. Mean ± s.e.m. One-way ANOVA; *, p<0.05, ns, not significant.

Next, we investigated whether $(GR)_{100}$- or $(PR)_{100}$-mCherry induces ER stress. As shown in **Fig. 3c and d**, transient expression of $(GR)_{100}$- or $(PR)_{100}$-mCherry causes upregulation of phosphorylated IRE1 (pIRE1) and TRAF2 (pTRAF2), i.e., activated forms of IRE1 and TRAF2, as well as alternative splicing of XBP1 mRNA in U-2 OS cells, compared to the mCherry control, suggesting that R-DPRs activates IRE1 in these cells. Of note, 4μ8C, an inhibitor of both IRE1 kinase and endonuclease activities (Cross et al., 2012), dose-dependently suppresses pJNK levels in U-2 OS cells expressing $(GR)_{100}$- or $(PR)_{100}$-mCherry (**Fig. 3e**), suggesting that R-DPRs activate JNK via IRE1.

Inhibiting JNK or IRE1 activity suppresses R-DPR-induced SG formation in U-2 OS cells

SGs play a critical role in R-DPR-mediated cytotoxicity. Indeed, R-DPRs can induce poorly dynamic SGs in cultured cells without additional stress (Boeynaems et al., 2017; K. H. Lee et al., 2016). When expressed in U-2 OS cells for 48 hours, $(GR)_{100}$- or $(PR)_{100}$-mCherry respectively causes ~70% or ~30% cells to exhibit SGs, as indicated by immunofluorescent staining of G3BP1 and TIA1, two SG markers (**Fig. 4** and **Supplementary Fig. 2**). Furthermore, treating the cells with 50 μM of SP600125 for 24 hours or 4μ8C for six hours significantly decreases the percent of cells exhibiting SGs, but not R-DPR protein levels (**Fig. 4** and **Supplementary Fig. 2**), suggesting that IRE1/JNK promotes R-DPR-induced SG assembly.

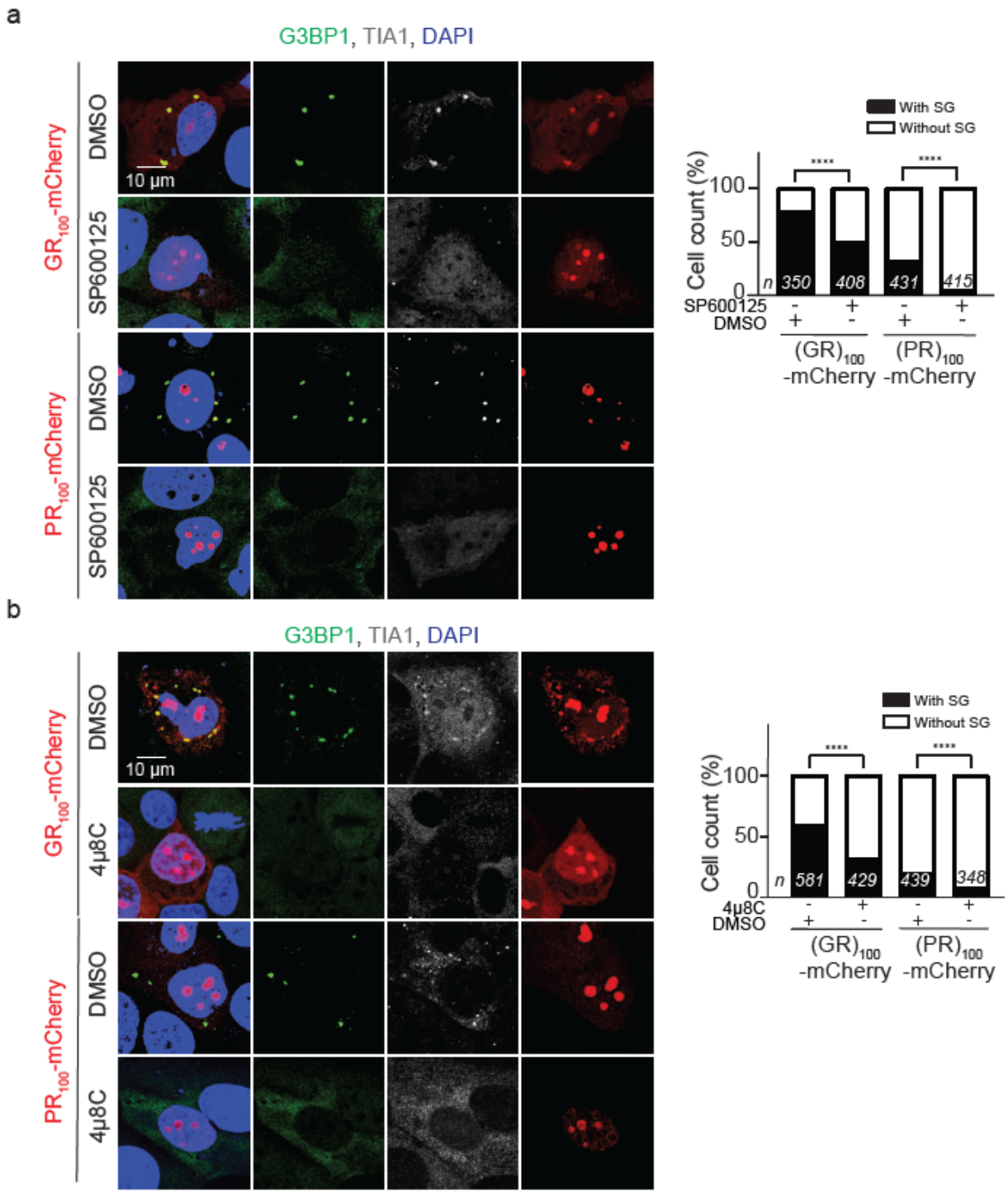

Figure 4: ER stress and JNK promote R-DPR-induced SG assembly in U-2 OS cells. U-2 OS cells expressing (GR/ PR)$_{100}$-mCherry (red) treated with DMSO, 50 µM SP600125, or 50 µM 4µ8C and stained with G3BP1 (green), TIA1 (white), and DAPI (blue). Quantification showing percent of cells with or without SGs. χ2-test; ****: p<0.0001.

G3BP1 plays a critical role in SG assembly, as its knockdown strongly reduces SG formation caused by a variety of stressors, whereas its overexpression induces SG formation without additional stress (Kedersha et al., 2016). In addition, we and others found that double-knockout of G3BP1 and its homolog, G3BP2, completely abolishes R-DPR-induced SGs (Boeynaems et al., 2017; K. Zhang et al., 2018). Here, we show that a 24- or six-hour treatment of SP600125 or 4μ8C, respectively, strongly decreases G3BP1 levels in cells expressing $(GR)_{100}$- or $(PR)_{100}$-mCherry (**Fig. 5a and b**), suggesting that JNK inhibition downregulates G3BP1. In addition, we found that these inhibitors decrease G3BP2, but not TIA1, levels (**Fig. 5a**), suggesting that JNK regulates some SG proteins.

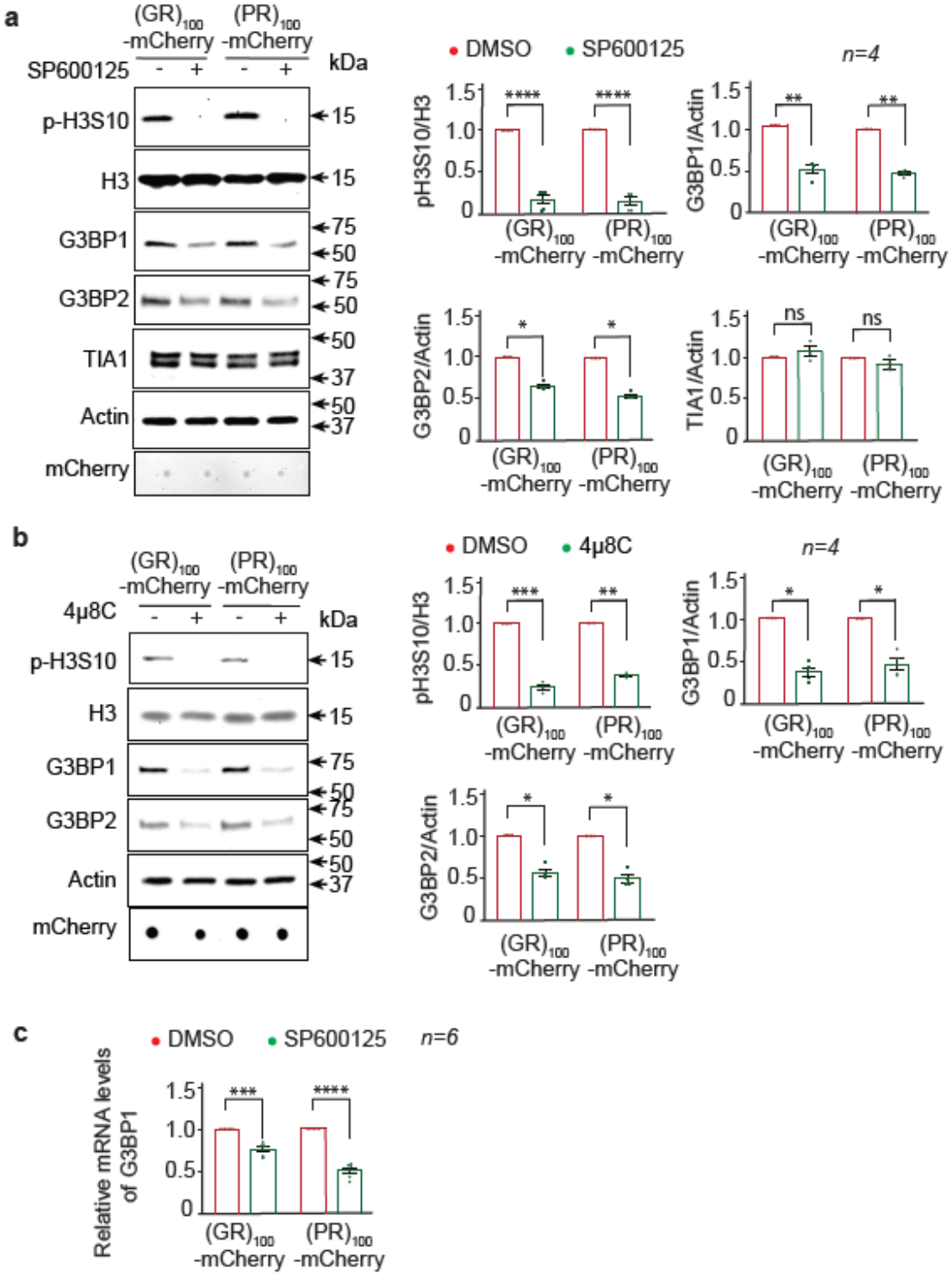

Figure 5: JNK promotes G3BP1 expression and H3S10 phosphorylation in U-2 OS cell expressing R-DPRs. Western or dot (for mCherry only) blots of lysates from U-2 OS cells expressing $(GR/PR)_{100}$-mCherry, treated with DMSO or (a) 50 μM SP600125 and (b) 50 μM

4μ8C. (c) Relative levels of G3BP1 mRNA as compared to GAPDH from U-2 OS cells expressing $(GR/PR)_{100}$-mCherry, treated with DMSO or 50 μM SP600125. Mean ± s.e.m. Student's t-tests; ****, $p<0.0001$; ***, $p<0.001$; **, $p<0.01$; *, $p<0.05$; ns, not significant.

A U-2 OS cell line stably expressing GFP-tagged G3BP1 (G3BP1-GFP) under the control of a lentiviral promoter is widely used to study SG biology (Figley, Bieri, Kolaitis, Taylor, & Gitler, 2014). We found that SP600125 suppresses the level of endogenous G3BP1, but not G3BP1-GFP, in these cells when transfected with $(GR)_{100}$- or $(PR)_{100}$-mCherry (**Supplementary Fig. 3**), possibly because the regulation of JNK on G3BP1 relies on the genomic promoter of *G3BP1*. If this is the case, JNK inhibition likely suppresses *G3BP1* transcription. Indeed, as shown in **Fig. 5c**, SP600125 significantly decreases *G3BP1* mRNA levels in U-2 OS cells expressing $(GR)_{100}$- or $(PR)_{100}$-mCherry, suggesting that JNK regulates G3BP1 at the transcriptional level in these cells.

Widely used in SG studies, sodium arsenite induces ER stress and SG assembly within an hour (Anderson & Kedersha, 2008; Cheng et al., 2018; Wheeler, Matheny, Jain, Abrisch, & Parker, 2016; P. Yang et al., 2020). To test whether JNK also plays a role in arsenite-induced SG formation, we co-treated U-2 OS cells with 0.5 mM sodium arsenite and 50 μM of SP600125 for an hour. As shown in **Supplementary Fig. 4**, SP600125 suppresses the pJNK level, but not the percentage of SG-positive cells, suggesting that JNK does not contribute to SG assembly caused by one-hour arsenite stress. Consistent with these data, cellular G3BP1 levels are unaltered in these cells, suggesting that one-hour JNK inhibition is insufficient to affect G3BP1 protein levels or SG assembly.

A prior study showed that in mouse differentiating neurons, activated JNKs in the nucleus are enriched in the promoter regions of certain genes, including G3BP1, where they phosphorylate certain chromatin components i.e., histone 3 protein at Serine10 position (H3S10) (Tiwari et al.,

2011). As H3S10 phosphorylation (pH3S10) causes the chromatin to adopt an "open" chromatin structure, which activates transcription (Allis & Jenuwein, 2016; Rossetto, Avvakumov, & Cote, 2012; Stricker, Koferle, & Beck, 2017), one possible mechanism by which JNK regulates *G3BP1* transcription is via pH3S10. Consistent with this notion, a 24- or six-hour treatment of SP600125 or 4μ8C, respectively, strongly suppresses pH3S10 levels in U-2 OS cells expressing $(GR)_{100}$- or $(PR)_{100}$-mCherry **(Fig. 5a and b)**.

Inhibiting IRE1/JNK activity suppresses neurotoxicity in c9ALS/FTD patient-derived iPSNs

To validate our findings in a patient-relevant model, we used iPSC-derived neurons (iPSNs) derived from c9ALS/FTD patients. While these iPSNs rarely exhibit SGs under non-stressed conditions, we previously showed that they are constitutively under a low level of stress, as indicated by a mild increase in the phospho-eIF2α. In addition, SG inhibitors GSK2606414 and ISRIB, which suppress R-DPR-induced SG formation, suppress subcellular defects in these iPSNs, suggesting that SG assembly contributes to the iPSN toxicity (K. Zhang et al., 2018).

Compared to control iPSNs, c9ALS/FTD iPSNs do not exhibit a strong phenotype or reduced survival under non-stressed conditions but are more sensitive to a variety of stressors, including the ER stressor tunicamycin (Donnelly et al., 2013; Haeusler et al., 2014; Shi et al., 2018). We show that a 24-hour treatment of five μM tunicamycin (TM) causes cell death, as indicated by propidium iodide (PI) staining, in four different c9ALS/FTD iPSN lines, which is suppressed by co-treatments of either SP600125 or 4μ8C (**Fig. 6a and Supplementary Fig. 5**). Consistent with these data, we show that the G3BP1 level in the c9ALS/FTD iPSNs increases upon tunicamycin treatment, which is suppressed by SP600125 and 4μ8C **(Fig. 6b)**. Together, these data suggest that inhibiting IRE1/JNK activity suppresses neurotoxicity and the G3BP1 level in c9ALS/FTD iPSNs.

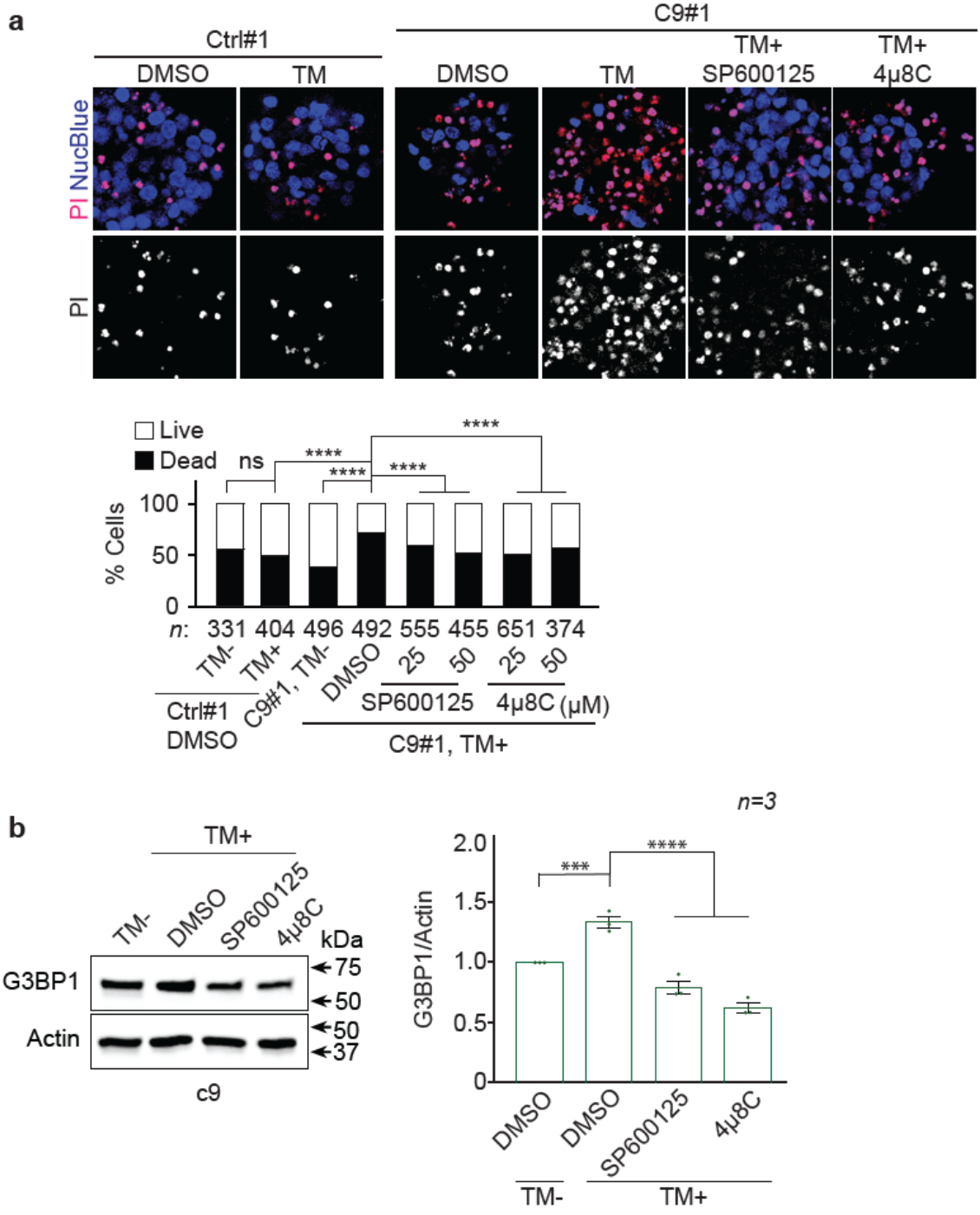

Figure 6: Inhibition of JNK or ER stress suppresses toxicity in c9ALS/FTD iPSNs. (a) Control (Ctrl) or c9ALS/FTD (c9) Line #1 iPSNs treated with 5 μM tunicamycin (TM) together with DMSO, SP600125, or 4μ8C and stained with propidine iodide (PI, dead cells) and NucBlue (all cells). Quantification shows the percent of live and dead cells. $\chi 2$-test. Mean ± s.e.m. One-way ANOVA with Dunnett's test; ****: $p<0.0001$. (b) Western blot of c9 lysates treated with 5 μM tunicamycin (TM) together with DMSO, JNK inhibitor SP600125, or IRE1 inhibitor 4μ8C. Mean ± s.e.m. Student's t-tests; ****, $p<0.0001$; ***, $p<0.001$.

Loss of G3BP/Rin suppresses neurodegeneration in c9ALS/FTD fly models

Previously, we showed that G3BP1/2 double KO abolishes R-DPR-induced cellular defects in U-2 OS cells and SG inhibitors GSK2606414 and ISRIB suppress $(G_4C_2)_{30}$-mediated eye degeneration in flies (K. Zhang et al., 2018), suggesting that inhibiting SG formation suppresses c9ALS/FTD-related cytotoxicity or neurodegeneration. Given the importance of G3BP1 and 2 in SG assembly, we postulate that loss of G3BP also suppresses neurodegeneration. In flies, *rin* is the only homolog of mammalian *G3BP1* and *2*. Here, we show that a loss of function *rin* mutation heterozygously suppresses eye degeneration caused by $(G_4C_2)_{30}$, $(GR)_{36}$, or $(PR)_{36}$ (**Fig. 7**), suggesting that loss of G3BP/Rin suppresses neurodegeneration in fly models of c9ALS/FTD.

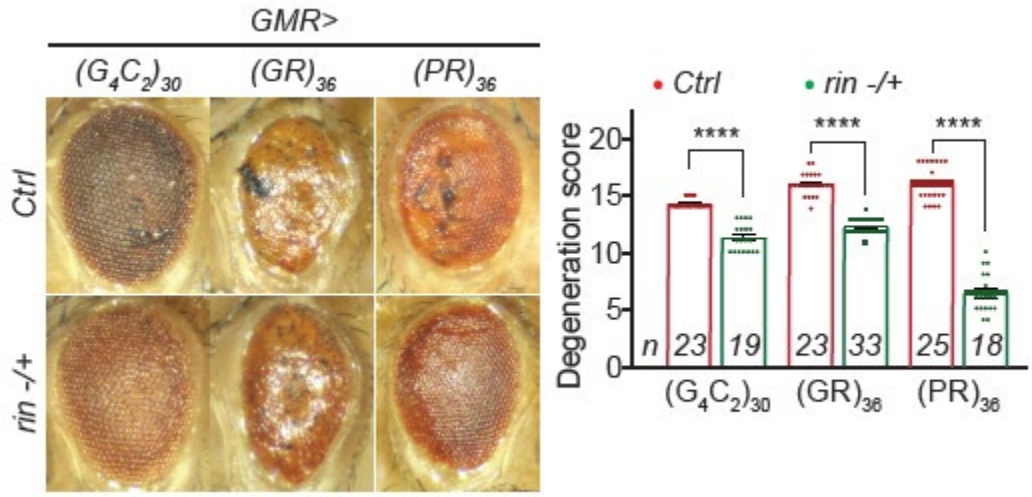

Figure 7: Loss of G3BP1/rin suppresses eye degeneration in c9ALS/FTD fly models. Fly eyes expressing $(G_4C_2)_{30}$, $(GR)_{36}$, or $(PR)_{36}$, without (Ctrl) or with heterozygous loss of function of *rin*. Mean ± s.e.m. Student's t-tests; ****, $p<0.0001$.

Discussion

Despite the importance of SGs in ALS/FTD pathogenesis, it is unclear how SG assembly is regulated at the cellular level and whether this regulation is related to pathomechanism. Here, we show that the ER stress/IRE1/JNK axis promotes SG formation caused by R-DPRs and contributes

to neurodegeneration in animal and cellular models of c9ALS/FTD. Mechanistically, activated JNK promotes the *G3BP1* transcription, likely by phosphorylating H3S10, thereby increasing the G3BP1 protein level (**Fig. 8**). Together, our findings suggest a novel pathway regulating SG formation, which contributes to ALS/FTD pathogenesis.

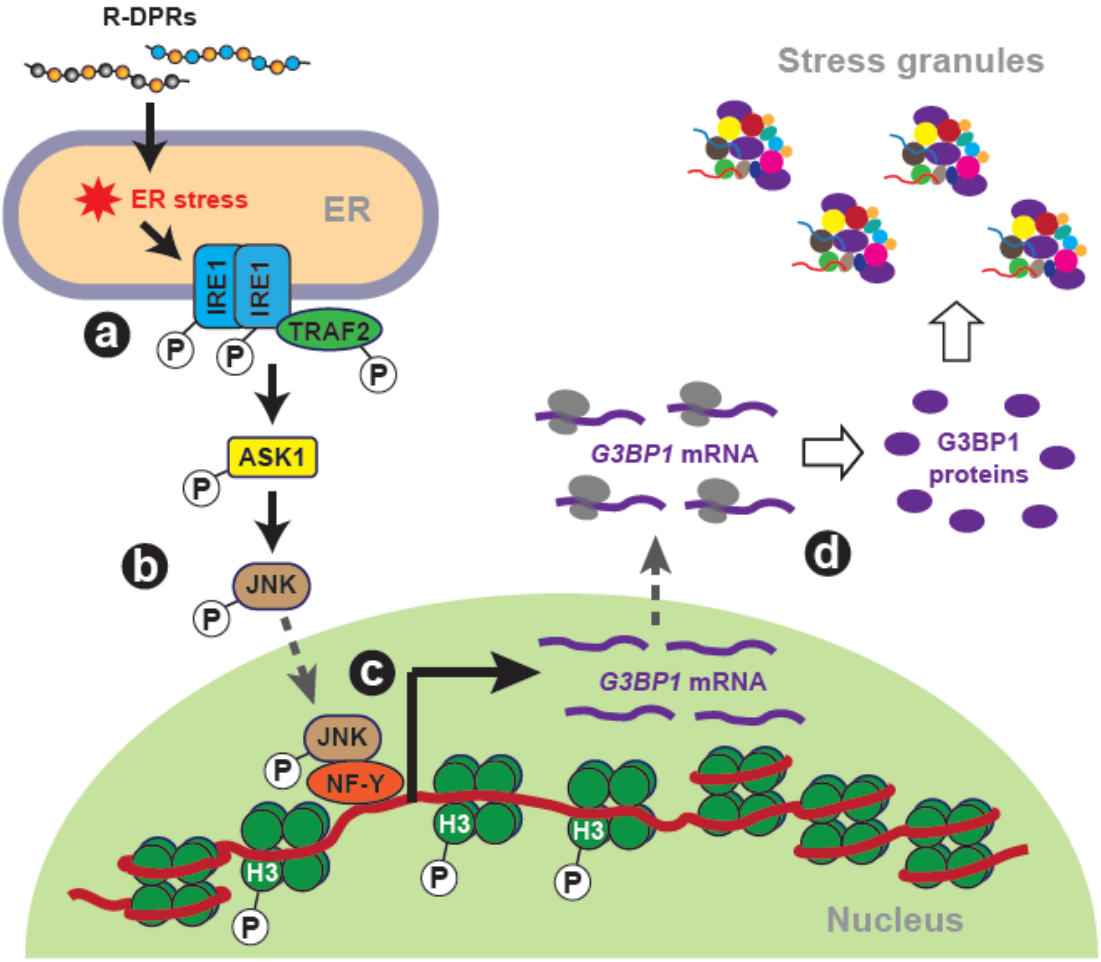

Figure 8: Schematic representation of ER stress/JNK promoting SG assembly in c9ALS/FTD. (a) R-DPRs induce ER stress, activating IRE1 and TRAF2. (b) Activated IRE1/TRAF2 complex activates ASK1, which subsequently activates JNK via phosphorylation. (c) Activated JNK translocates to the nucleus and, together with NF-Y, localizes to the promoter region of *G3BP1*, where it phosphorylates H3 at Serine10. H3S10 phosphorylation relaxes DNA, allowing NF-Y-mediated transactivation of *G3BP1*. (d) G3BP1 protein level is upregulated, causing SG assembly.

How JNK promotes G3BP1 transcription is unclear. A previous study showed that in mice neurons, the transcription factor complex nuclear factor Y (NF-Y) and active JNK are recruited to

promoter regions of some genes, including *G3BP1* (Tiwari et al., 2011), where activated JNK phosphorylates H3S10, thereby allowing NF-Y-mediated *G3BP1* transactivation (**Fig. 8**). Future studies can test this model in U-2 OS and iPSN models of c9ALS/FTD.

When overexpressed, R-DPRs induce SGs in cells over a 24-48 hour period (Boeynaems et al., 2017; K. H. Lee et al., 2016) (and **Fig. 4** and **Supplementary Fig. 2**), whereas many stressors, e.g., arsenite, induces SGs within an hour. Previous studies on SG assembly mechanisms mostly focus on the latter, i.e., SGs induced by short-term stress (Jain et al., 2016; Kedersha et al., 2016; P. Yang et al., 2020). Some of the identified mechanisms are verified in SGs induced by long-term stress, e.g., eIF2α phosphorylation is required in both arsenite and R-DPR-induced SG formation (Boeynaems et al., 2017; K. Zhang et al., 2018). However, the uniqueness of long-term-stress-induced SG formation is unclear. Here, we show that JNK promotes SG formation induced by R-DPRs, but not one-hour treatment of arsenite, suggesting a mechanism specifically for long-term-stress-induced SG formation. This specificity likely comes from the ability of JNK to cause transcriptional changes, which, compared to posttranslational modifications, are more likely implicated in long-term stress responses (Q. Zhang et al., 2015).

Previous studies identified critical roles of the MAPK/JNK pathway in stress responses and neurodegeneration, including ALS. It induces apoptosis in a mouse model of SOD1-mediated ALS (S. Lee et al., 2016), causes energy deficiencies in a mouse model of Wallerian degeneration (J. Yang et al., 2015), and disrupts lipid metabolism due to mitochondrial oxidative stress in fly and mouse models (L. Liu et al., 2015). Our finding that JNK promotes SG formation in cellular models of c9ALS/FTD identifies a novel route by which this pathway contributes to stress responses and neurodegeneration, suggesting a broader role of MAPK/JNK.

In addition to the MAPK/JNK pathway, other pathways and processes are also known to contribute to SG formation, and targeting some of these pathways/processes suppresses neurodegeneration or cytotoxicity in ALS/FTD models (Becker et al., 2017; Gilks et al., 2004; Jain et al., 2016; Kedersha et al., 2016; Kedersha et al., 2008; Ohn et al., 2008; K. Zhang et al., 2018). However, the complex network regulating SG formation in cells is far from understood. Mass spectrometry analyses identified ~400 proteins in yeast and mammalian SGs (Jain et al., 2016), and genetic screens identified more than 300 genes whose loss limits or reduces arsenite-induced SG formation in U-2 OS cells (Ohn et al., 2008; P. Yang et al., 2020). For most of these proteins/genes, how they contribute to SG formation and whether they are implicated in ALS/FTD pathogenesis is unclear. Future studies addressing these questions will provide a better understanding of SG biology and potentially identify novel therapeutic targets for the diseases.

Materials and Methods

IPSC culture and motor neuron differentiation

IPSC lines from C9orf72 patients and non-neurological controls were obtained from Cedars-Sinai Stem cell Core (patient demographics are provided in **Supplementary Table 1**). IPSCs were differentiated into direct induced motor neurons (diMNs) using a previously published protocol (A. N. Coyne et al., 2020). Briefly, iPSCs were grown in mTeSR media on Matrigel (Corning)-coated 10 cm dishes for two weeks before differentiation. At 40% confluency, iPSC colonies were cultured in Stage 1 media containing IMDM 47.5% (Gibco), 47.5% F12, 1% NEAA (Gibco), 1% Pen/Strep (Gibco), 2% B27 (Gibco), 1% N2 (Gibco), 0.2 µM LDN193189 (Stemgent), 10 µM SB431542 (StemCell Technologies), and 3 µM CHIR99021 (Sigma Aldrich) for six days. On Day 6, colonies were passaged with accutase (EMD Millipore) and re-plated on Matrigel-coated 6-well

plates. Cells were cultured in Stage 2 media containing IMDM 47.5% (Gibco), 47.5% F12, 1% NEAA (Gibco), 1% Pen/Strep (Gibco), 2% B27 (Gibco), 1% N2 (Gibco), 0.2 µM LDN193189 (Stemgent), 10 µM SB431542 (StemCell Technologies), and 3 µM CHIR99021 (Sigma Aldrich), 0.1 µM all-trans RA (Sigma Aldrich), and 1 µM SAG (Cayman Chemicals) until Day 12. On day 12, cells were trypsinized (GenClone) and replated on Matrigel-coated 24-well plates for imaging or 6-well plates for biochemistry. Cells were cultured in Stage 3 media containing IMDM 47.5% (Gibco), 47.5% F12, 1% NEAA (Gibco), 1% Pen/Strep (Gibco), 2% B27 (Gibco), 1% N2 (Gibco), 0.1 µM Compound E (Millipore), 2.5 µM DAPT (Sigma Aldrich), 0.1 µM db-cAMP (Millipore), 0.5 µM all-trans RA (Sigma Aldrich), 0.1 µM SAG (Cayman Chemicals), 200 ng/mL Ascorbic Acid (Sigma Aldrich), 10 ng/mL BDNF (PeproTech), 10 ng/mL GDNF (PeproTech) until day 32. All cells were maintained at 37°C and 5% CO_2.

Propidium iodide (PI) staining

Day 32 diMNs were treated with 1 µg/mL of PI (Invitrogen) and one drop of NucBlue (Invitrogen) along with the media and incubated at 37°C and 5% CO_2 for 30 min. Images were acquired using a Zeiss LSM 900 confocal microscope (Carl Zeiss) with an Axiocam 512 color camera and related software. For each condition, 10-15 images were taken.

***Drosophila* genetics**

Drosophila were raised on yeast-cornmeal-molasses food at 25°C. All RNAi fly stocks were procured from Bloomington Drosophila Stock Centre.

For eye degeneration assay, *GMR-Gal4, UAS-$(G_4C_2)_{30}$/CyO* were crossed to Canton-S flies or *UAS-RNAi,* and *GMR-Gal4, UAS-$(G_4C_2)_{30}$/+; UAS-RNAi (II or III)* and *GMR-Gal4, UAS-30R/+* were selected and aged at 27°C for 12 days. The external morphology of degenerated eyes was

scored using a previously published method (G. P. Ritson et al., 2010). Briefly, points were added for necrotic patches, loss of bristles, retinal collapse, loss of ommatidial structure, and depigmentation of the eye. Both the eyes were scored and the individual scores were combined to give a total 'degeneration score' in the range of 0-20. Eye images were captured using a ZEISS SteREO Discovery.V8 microscope (Carl Zeiss) with Axiocam 512 color camera and related software.

For the lethality assay, male flies from *OK371-Gal4*; *UAS-$(G_4C_2)_{30}$/Gal80, TM6* were crossed to virgin female Canton-S or *UAS-RNAi* flies at 25°C, and parent flies were removed after three days. After 15 days, non-tubby offspring, i.e. *OK371-Gal4/+; UAS-$(G_4C_2)_{30}$/+; UAS-RNAi (II/III)/+*, was scored as either fully eclosed (live) or pharate lethal (unable to eclose).

For *bsk/JNK* activity in flies, male flies from *OK371-Gal4 or OK371-Gal4; UAS-$(G_4C_2)_{30}$/Gal80, TM6* were crossed to virgin female flies from *puc-LacZ/TM6*. Third instar larvae of the offspring *OK371-Gal4/+; +/puc-LacZ or OK371-Gal4/+; UAS-$(G_4C_2)_{30}$/puc-LacZ* were collected and their ventral nerve cords were dissected and subsequently stained.

For Xbp1-EGFP expression in flies, male flies from *OK371-Gal4* or *OK371-Gal4*; *UAS-$(G_4C_2)_{30}$/Gal80, TM6* were crossed to virgin female flies from *Xbp1-EGFP*. Third instar larvae of the offspring *OK371-Gal4/+; +/Xbp1-EGFP* or *OK371-Gal4/+; UAS-$(G_4C_2)_{30}$/Xbp1-EGFP*) were collected and VNC was dissected and stained.

Cell culture

U2-OS cells (ATCC, HTB-96) were grown in DMEM (Gibco) supplemented with 10% fetal bovine serum (Gibco) and 1% penicillin-streptomycin and maintained at 37°C in a humidified incubator supplemented with 5% CO_2. Transfections were performed using Lipofectamine 3000

(Invitrogen) reagent as per the manufacturer's protocol. 48 h post-transfection, cells were either fixed and immunostained or lysed for immunoblot.

Immunofluorescent staining

Fly VNCs were fixed with 3.7% formaldehyde for 20 minutes and penetrated in 0.4% PBX (PBS with 0.4% Triton X-100) for 1 hr at room temperature. Tissues were stained with primary antibodies anti-LacZ (DHSB, 40-1a, AB_528100,) and anti-elav (DHSB, 7E8A10) in 0.4% PBX and 10% donkey serum (DS) overnight. After that, VNCs were washed three times in 0.4% PBX (20 min each) and incubated with secondary antibodies conjugated to Alexa Fluor 488 and 568 (Thermo Scientific) in 0.4% PBX containing 10% DS. All primary antibodies were used at 1:200 dilutions and secondary antibodies were used at 1:1000 dilutions. Tissues were washed three times with 0.4% PBX (20 min each) and mounted on a coverslip using Prolong antifade Gold mountant (Invitrogen) along with DAPI.

U-2 OS cells or iPSNs were fixed with 4% paraformaldehyde for 20 min followed by penetration in 0.1% PBX (PBS with 0.1% Triton X-100) for 20 min at room temperature. For iPSNs, 0.3% PBX was used. Cells were blocked with 3% donkey serum (DS) followed by overnight incubation with primary antibodies in 0.1% TBST (TBS with 0.1% Tween-20) containing 3% DS. Primary antibodies were used as follows: G3BP1 (Abcam, 181149), G3BP2 (ProteinTech, 16276-1-AP, AB_2878237) and TIA1 (ProteinTech, 12133-2-AP, AB_2201427), at 1:200 dilutions. Cells were washed three times with TBST (20 min each) followed by incubation with secondary antibodies conjugated to either Alexa Fluor 488, 568, or 647 (1:1000 dilution) in TBST and 3% DS. After that, cells were washed thrice with TBST (20 min each) and mounted using Prolong antifade Gold mountant (Thermo Scientific).

Images were acquired using Zeiss LSM900 confocal microscope (Carl Zeiss) with an Axiocam 512 color camera and related software.

Plasmid source and construction

The mCherry plasmid was procured from Addgene, and $(GR)_{100}$-mCherry was a gift from Dr. Yong-Jie Zhang (Cook et al., 2020). To generate the mCherry-tagged poly-PR expression plasmid, the BioID sequence in myc-BioID-(PR)x100(F. L. Liu et al., 2022) was replaced with a NdeI/BamHI fragment encoding mCherry followed by a flexible linker (mCherry-GGGSx3).

Drug treatments

U2-OS cells were treated with JNK inhibitor SP600125 (50 μM) (Selleck Chemicals) for 24 h or with IRE1 inhibitor 4μ8C (50 μM) (Selleck Chemicals) for 6 h and incubated at 37°C.

For iPSNs, day 32 diMNs were stressed with 5 μM of tunicamycin (Sigma Aldrich) and co-treated with either DMSO or 25-50 μM JNK inhibitor (SP600125) or 25-50 μM IRE1 inhibitor (4μ8C) for 24 h.

Western blot, immunoblot

U2-OS and iPSNs were lysed in Laemmli buffer and heated to 98℃ for 15 min. The protein samples were separated using 4-15% SDS mini-PROTEAN TGX precast gels (Bio-Rad) and transferred to 0.45 μm nitrocellulose membranes (Bio-Rad). For dot blots, samples were directly blotted on the nitrocellulose membrane and air-dried for 20 min. Blots were blocked with 5% milk for 1 hr and incubated overnight with the primary antibody (1:1000 dilution, for actin 1:5000) in 0.1% TBST containing 5% milk. Primary antibodies were used as follows: JNK (Cell Signaling, 9252S, AB_2250373,), phospho-JNK (Cell Signaling, 9251S, AB_331659), H3 (Cell signaling,

9715S, AB_331563,), phospho-H3S10 (Cell Signaling, 9706S, AB_331748), IRE1 (Cell Signaling, 3294S, AB_823545,), phospho-IRE1 (Abcam, ab48187, AB_873899), TRAF2 (Cell Signaling, 4724S, AB_2209845,), phospho-TRAF2 (Cell signaling, 13908S, AB_2798342), G3BP1 (Abcam, 181149), G3BP2 (ProteinTech, 16276-1-AP, AB_2878237) and TIA1 (ProteinTech, 12133-2-AP, AB_2201427) at 1:1000 dilutions and actin (EMD Millipore, MAB1501, AB_2223041,), mCherry (Abcam, ab167453, AB_2571870,) at 1:5000 dilutions. Blots were washed with TBST followed by incubation with HRP conjugated secondary antibodies in TBST and 5% milk (1:5000 dilution). For mCherry dot blots, bovine serum albumin (BSA) was used for blocking instead of milk. Chemiluminescent substrate WesternLigtning Plus-ECL (PerkinElmer) was used for detection. Images were captured using the iBright™ FL1500 Imaging system (Thermo Fischer Scientific).

MTT assay

U2-OS cells were incubated with media containing MTT (1 mg/mL) at 37°C for 4 h. After that, media was removed and cells were lysed using DMSO, and absorbance was measured at 570 nm using A Tecan Spark multimode microplate reader.

PCR

RNA was isolated from cells using Trizol reagent (Invitrogen) following the manufacturer's protocol. Reverse transcription was done using the SuperScript IV First-Strand Synthesis kit (Invitrogen). Quantitative PCR was done using SYBR-Green Master mix using Applied Biosystem Quant Studio 7. Following primers were used: for *GAPDH* forward 5'-GTTCGACAGTCAGCCGCATC-3', reverse 5'-GGAATTTGCCATGGGTGGA3-'; for *G3BP1* forward 5'-GTCCTTAGCAACAGGCCCAT-3', reverse 5'-TTATCTCGTCGGTCGCCTTC-3'.

To analyze *XBP1* alternative splicing events, cDNA was amplification using DreamTaq PCR mix (Invitrogen) and separated on 2.5% agarose gel (MetaPhor agarose, Lonza). Following primers were used: *XBP1* forward 5'-TTACGAGAGAAAACT CATGGC-3', reverse 5'- GGGTCCAAG TTGTCCAGAATG C-3'.

Quantification and Statistical analysis

Western blots were quantified using FIJI-just ImageJ. For SG counts and PI staining, at least 300 cells were counted. The data are presented as Mean ± SEM. Statistical analysis was done using paired or unpaired Student's t-test, one-way ANOVA with Dunnett's test, and Chi-square test using GraphPad Prism version 8 (GraphPad) as described in figure legends. $* p < 0.05$, $** p < 0.01$, $*** p < 0.001$, $*** p < 0.0001$.

Acknowledgments

We thank Yong-Jie Zhang and Karen Jansen-West for the constructs. Bloomington Drosophila Stock Center (NIH P40OD018537, fly stocks). Funding support: K.Z., NIH-NINDS/NIA (R01NS117461), DoD (W81XWH-21-1-0082), Target ALS, and the Frick Foundation for ALS.

Competing interests

The authors declare no competing interests.

Supplementary figures:

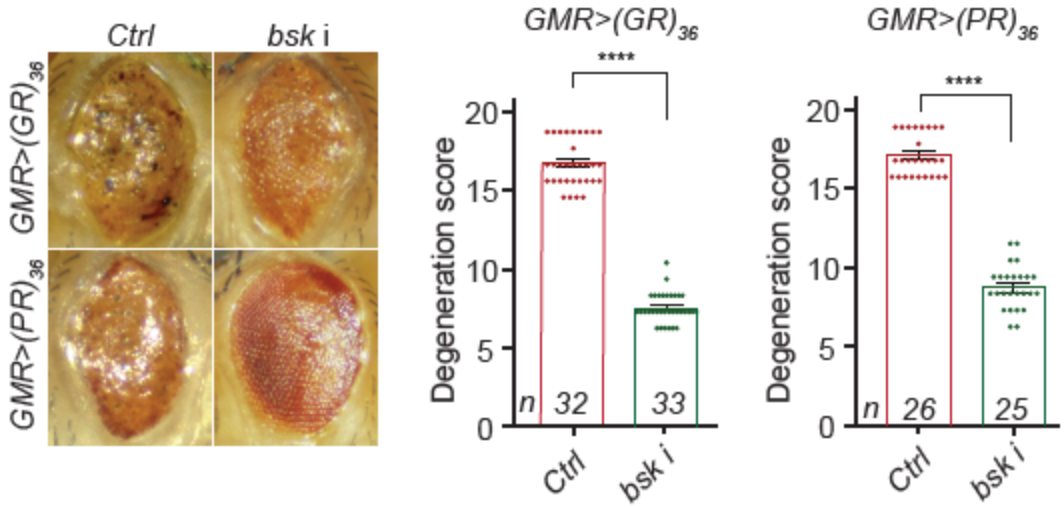

Supplementary figure 1: Loss of *bsk* suppresses R-DPR-mediated eye degeneration in flies. Fly eyes expressing $(GR)_{36}$ or $(PR)_{36}$ using GMR-GAL4, without (control, Ctrl) or with co-expressing *bsk* i. Student's t-test; ****: $p<0.0001$

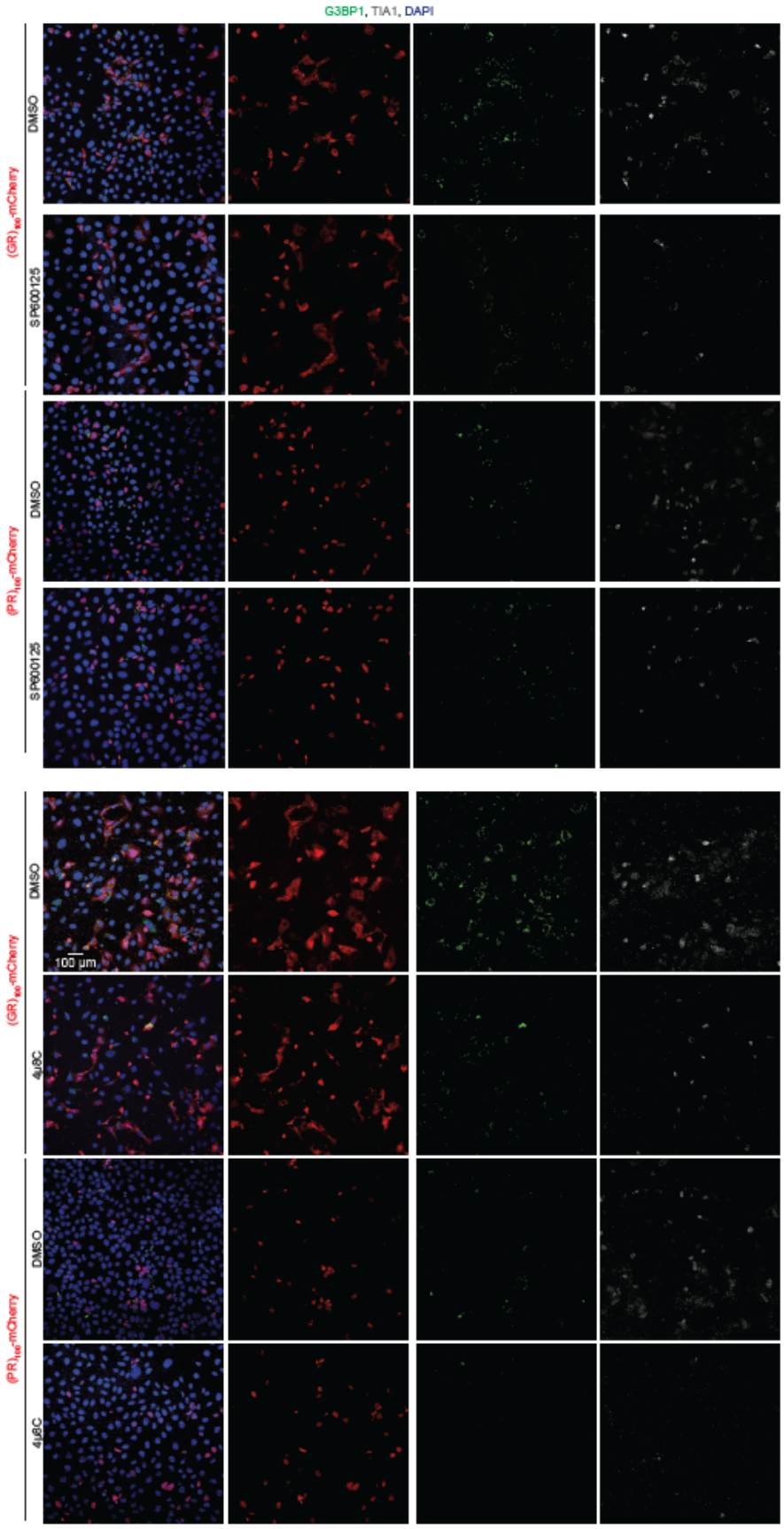

448

Supplementary figure 2: Large views of Fig. 4. U-2 OS cells expressing $(GR/PR)_{100}$-mCherry (red) treated with DMSO, 50 µM SP600125, or 50 µM 4µ8C and stained with G3BP1 (green), TIA1 (white), and DAPI (blue).

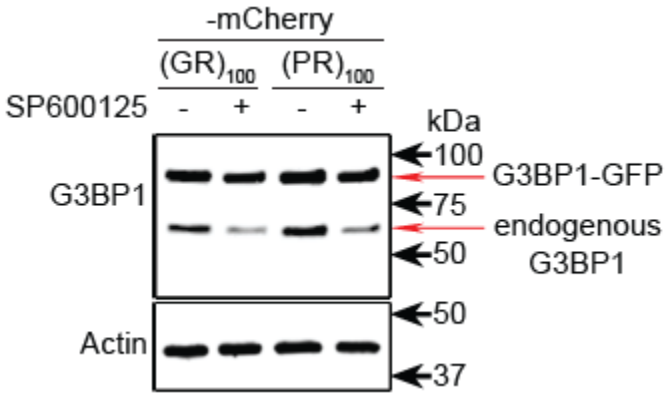

Supplementary figure 3: JNK regulates endogenous G3BP1. Western blots of lysates from U-2 OS cells stably expressing a G3BP1-GFP under a lentiviral promoter and transiently expressing $(GR/PR)_{100}$-mCherry, treated with DMSO or 50 µM inhibitor SP600125.

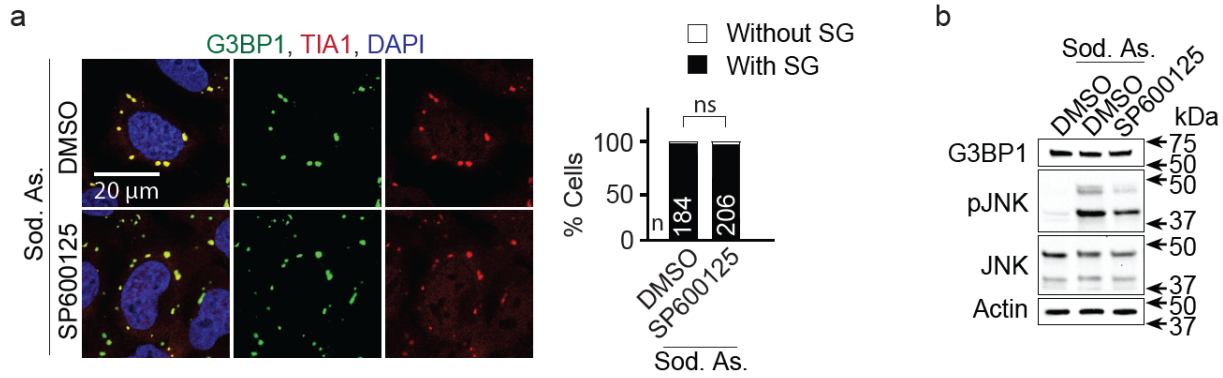

Supplementary figure 4: JNK does not promote arsenite-induced SG formation. (a) U-2 OS cells treated with 0.5 mM sodium arsenite (Sod. As.) together with DMSO or 50 µM SP600125 for 1 h and stained with G3BP1 (green), TIA1 (red), and DAPI (blue). Quantification shows percent of cells with or without SGs. Mean ± s.e.m. χ2-test. ns, not significant. (b) Western blots of lysates from U-2 OS cells treated with 0.5 mM sodium arsenite together with DMSO or 50 µM SP600125 for 1 h.

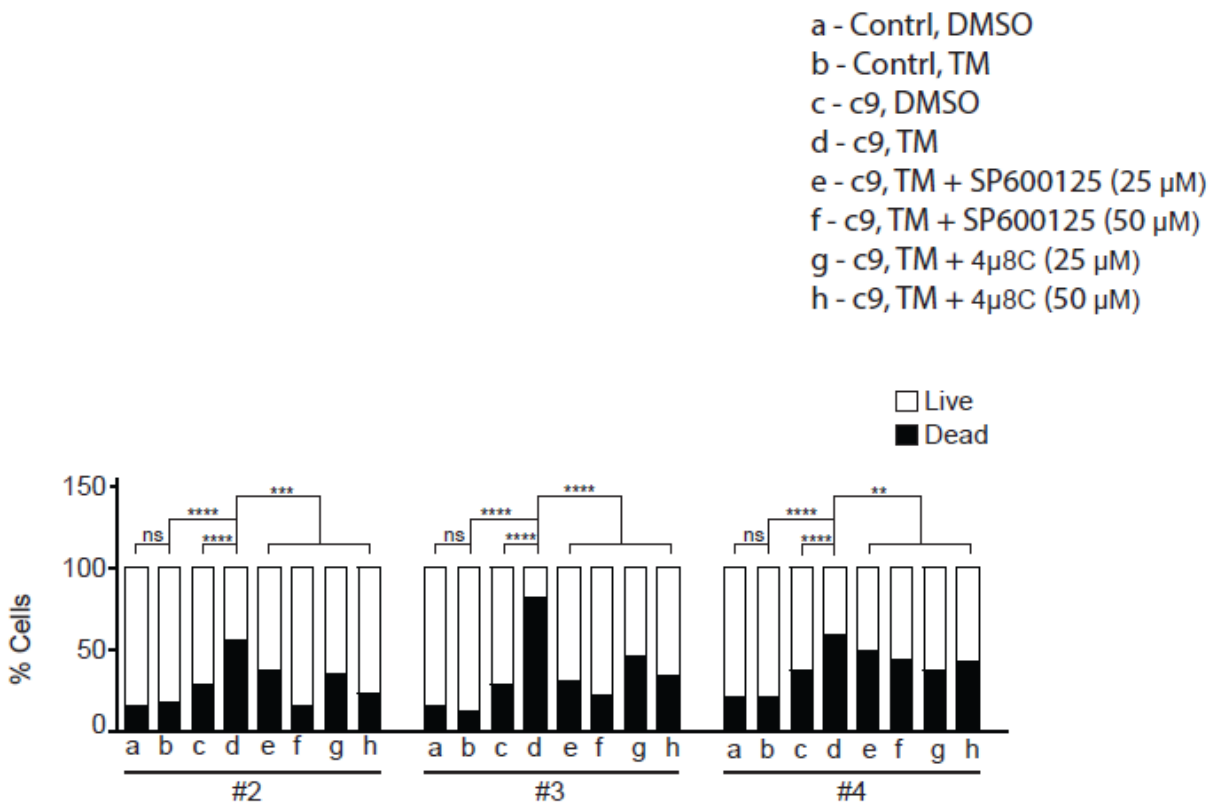

Supplementary figure 5: Inhibition of JNK or ER stress suppresses toxicity in multiple c9ALS/FTD iPSN lines. Control (Ctrl) or c9ALS/FTD (c9) Line #2, #3 and #4 iPSNs treated with 5 µM tunicamycin (TM) together with DMSO, SP600125, or 4µ8C and stained with propidine iodide (PI, dead cells) and NucBlue (all cells). Quantification shows percent of live and dead cells. $\chi 2$-test. ****: $p<0.0001$; ***: $p<0.001$; **: $p<0.01$; ns, not significant.

Supplementary Table 1: Demographics of patients whose iPSCs were used in this study

Cell line name	Source	Sex	Age at the time of collection	Disease/Type	Mutation	Origin
CS9XH7iCTR-nxx	Cedar Sinai	Male	53	Control	-	PBMC
CS8PAAiCTR-nxx	Cedar Sinai	Female	58	Control	-	PBMC
EDi036-A	Cedar Sinai	Female	79	Control	-	PBMC
EDi043-A	Cedar Sinai	Male	80	Control	-	PBMC
CS8KT3iALS-nxx	Cedar Sinai	Male	60	ALS	C9orf72 HRE	PBMC
CS7VCZiALS-nxx	Cedar Sinai	Male	64	ALS	C9orf72 HRE	PBMC
CS6ZLDiALS-nxx	Cedar Sinai	Female	Unknown	ALS	C9orf72 HRE	PBMC
CS0BUUiALS-nxx	Cedar Sinai	Female	63	ALS	C9orf72 HRE	PBMC

Figure legends for source data:

Figure 1-source data 1: Fly ventral nerve cord motor neurons expressing puc-lacZ without $(G_4C_2)_{30}$, stained with lacZ (red), Elav (a neuronal marker, green), and DAPI (blue).

Figure 1-source data 2: Magnified inner image of fly ventral nerve cord motor neurons expressing puc-lacZ without $(G_4C_2)_{30}$, stained with lacZ (red), Elav (a neuronal marker, green), and DAPI (blue).

Figure 1-source data 3: Fly ventral nerve cord motor neurons expressing puc-lacZ with co-expressing $(G_4C_2)_{30}$, stained with lacZ (red), Elav (a neuronal marker, green), and DAPI (blue).

Figure 1-source data 4: Magnified inner image of fly ventral nerve cord motor neurons expressing puc-lacZ with co-expressing $(G_4C_2)_{30}$, stained with lacZ (red), Elav (a neuronal marker, green), and DAPI (blue).

Figure 2-source data 1: Fly VNC motor neurons expressing Xbp1-GFP without $(G_4C_2)_{30}$, stained with Elav (a neuronal marker, red) and DAPI (blue).

Figure 2-source data 2: Fly VNC motor neurons expressing Xbp1-GFP with $(G_4C_2)_{30}$, stained with Elav (a neuronal marker, red) and DAPI (blue).

Figure 3-source data 1: U-2 OS cells expressing mCherry or $(GR/PR)_{100}$-mCherry (red) stained with pJNK (green) and DAPI (blue).

Figure 3-source data 2: Raw image of Western blots for lysates from U-2 OS cell expressing mCherry or $(GR/PR)_{100}$-mCherry showing actin

Figure 3-source data 3: Raw image of Western blots for lysates from U-2 OS cell expressing mCherry or $(GR/PR)_{100}$-mCherry showing IRE1

Figure 3-source data 4: Raw image of Western blots for lysates from U-2 OS cell expressing mCherry or $(GR/PR)_{100}$-mCherry showing p-IRE1

Figure 3-source data 5: Raw image of Western blots for lysates from U-2 OS cell expressing mCherry or $(GR/PR)_{100}$-mCherry showing TRAF2

Figure 3-source data 6: Raw image of Western blots for lysates from U-2 OS cell expressing mCherry or $(GR/PR)_{100}$-mCherry showing p-TRAF2

Figure 3-source data 7: Raw image of Western blots for lysates from U-2 OS cell expressing mCherry or $(GR/PR)_{100}$-mCherry showing JNK

Figure 3-source data 8: Raw image of Western blots for lysates from U-2 OS cell expressing mCherry or $(GR/PR)_{100}$-mCherry showing pJNK

Figure 3-source data 9: Raw image of Western blots for lysates from U-2 OS cell expressing mCherry or $(GR/PR)_{100}$-mCherry co-treated with DMSO or 4μ8C for 6 h showing actin

Figure 3-source data 10: Raw image of Western blots for lysates from U-2 OS cell expressing mCherry or $(GR/PR)_{100}$-mCherry co-treated with DMSO or 4μ8C for 6 h showing JNK

Figure 3-source data 11: Raw image of Western blots for lysates from U-2 OS cell expressing mCherry or $(GR/PR)_{100}$-mCherry co-treated with DMSO or 4μ8C for 6 h showing pJNK

Figure 5-source data 1: Raw image of Western blots of lysates from U-2 OS cells expressing $(GR/PR)_{100}$-mCherry, treated with DMSO or 50 μM SP600125 showing actin

Figure 5-source data 2: Raw image of Western blots of lysates from U-2 OS cells expressing $(GR/PR)_{100}$-mCherry, treated with DMSO or 50 µM SP600125 showing G3BP1

Figure 5-source data 3: Raw image of Western blots of lysates from U-2 OS cells expressing $(GR/PR)_{100}$-mCherry, treated with DMSO or 50 µM SP600125 showing G3BP2

Figure 5-source data 4: Raw image of Western blots of lysates from U-2 OS cells expressing $(GR/PR)_{100}$-mCherry, treated with DMSO or 50 µM SP600125 showing H3

Figure 5-source data 5: Raw image of Western blots of lysates from U-2 OS cells expressing $(GR/PR)_{100}$-mCherry, treated with DMSO or 50 µM SP600125 showing p-H3S10

Figure 5-source data 6: Raw image of Western blots of lysates from U-2 OS cells expressing $(GR/PR)_{100}$-mCherry, treated with DMSO or 50 µM SP600125 showing TIA1

Figure 5-source data 7: Raw image of Western blots of lysates from U-2 OS cells expressing $(GR/PR)_{100}$-mCherry, treated with DMSO or 50 µM 4µ8C showing actin

Figure 5-source data 8: Raw image of Western blots of lysates from U-2 OS cells expressing $(GR/PR)_{100}$-mCherry, treated with DMSO or 50 µM 4µ8C showing G3BP1

Figure 5-source data 9: Raw image of Western blots of lysates from U-2 OS cells expressing $(GR/PR)_{100}$-mCherry, treated with DMSO or 50 µM 4µ8C showing G3BP2

Figure 5-source data 10: Raw image of Western blots of lysates from U-2 OS cells expressing $(GR/PR)_{100}$-mCherry, treated with DMSO or 50 µM 4µ8C showing H3

Figure 5-source data 11: Raw image of Western blots of lysates from U-2 OS cells expressing $(GR/PR)_{100}$-mCherry, treated with DMSO or 50 µM 4µ8C showing p-H3S10

Figure 6-source data 1: Raw image of Western blot of c9 lysates treated with 5 µM tunicamycin (TM) together with DMSO, JNK inhibitor SP600125, or IRE1 inhibitor 4µ8C showing actin

Figure 6-source data 2: Raw image of Western blot of c9 lysates treated with 5 µM tunicamycin (TM) together with DMSO, JNK inhibitor SP600125, or IRE1 inhibitor 4µ8C showing G3BP1

Supplementary Figure 3-source data 1: Raw image of Western blots of lysates from U-2 OS cells stably expressing a G3BP1-GFP under a lentiviral promoter and transiently expressing $(GR/PR)_{100}$-mCherry, treated with DMSO or 50 µM inhibitor SP600125 showing G3BP1

Supplementary Figure 4-source data 1: U-2 OS cells treated with 0.5 mM sodium arsenite (Sod. As.) together with DMSO for 1 h and stained with G3BP1 (green), TIA1 (red), and DAPI (blue).

Supplementary Figure 4-source data 2: U-2 OS cells treated with 0.5 mM sodium arsenite (Sod. As.) together with 50 µM SP600125 for 1 h and stained with G3BP1 (green), TIA1 (red), and DAPI (blue).

Supplementary Figure 4-source data 3: Raw image for Western blots of lysates from U-2 OS cells treated with 0.5 mM sodium arsenite together with DMSO or 50 µM SP600125 for 1 h showing JNK

Supplementary Figure 4-source data 4: Western blots of lysates from U-2 OS cells treated with 0.5 mM sodium arsenite together with DMSO or 50 µM SP600125 for 1 h showing pJNK

Supplementary Figure 4-source data 5: Western blots of lysates from U-2 OS cells treated with 0.5 mM sodium arsenite together with DMSO or 50 µM SP600125 for 1 h showing G3BP1

References:

Allis, C. D., & Jenuwein, T. (2016). The molecular hallmarks of epigenetic control. *Nat Rev Genet, 17*(8), 487-500. doi:10.1038/nrg.2016.59

Anderson, P., & Kedersha, N. (2008). Stress granules: the Tao of RNA triage. *Trends Biochem. Sci, 33*(3), 141-150. doi:S0968-0004(08)00026-1 [pii];10.1016/j.tibs.2007.12.003 [doi]

Ash, P. E., Bieniek, K. F., Gendron, T. F., Caulfield, T., Lin, W. L., DeJesus-Hernandez, M., . . . Petrucelli, L. (2013). Unconventional translation of C9ORF72 GGGGCC expansion generates insoluble polypeptides specific to c9FTD/ALS. *Neuron, 77*(4), 639-646. doi:S0896-6273(13)00135-9 [pii];10.1016/j.neuron.2013.02.004 [doi]

Becker, L. A., Huang, B., Bieri, G., Ma, R., Knowles, D. A., Jafar-Nejad, P., . . . Gitler, A. D. (2017). Therapeutic reduction of ataxin-2 extends lifespan and reduces pathology in TDP-43 mice. *Nature, 544*(7650), 367-371. doi:nature22038 [pii];10.1038/nature22038 [doi]

Boeynaems, S., Bogaert, E., Kovacs, D., Konijnenberg, A., Timmerman, E., Volkov, A., . . . Van Den Bosch, L. (2017). Phase Separation of C9orf72 Dipeptide Repeats Perturbs Stress Granule Dynamics. *Mol. Cell, 65*(6), 1044-1055. doi:S1097-2765(17)30128-4 [pii];10.1016/j.molcel.2017.02.013 [doi]

Cheng, W., Wang, S., Mestre, A. A., Fu, C., Makarem, A., Xian, F., . . . Sun, S. (2018). C9ORF72 GGGGCC repeat-associated non-AUG translation is upregulated by stress through eIF2alpha phosphorylation. *Nat Commun, 9*(1), 51. doi:10.1038/s41467-017-02495-z

Cook, C. N., Wu, Y., Odeh, H. M., Gendron, T. F., Jansen-West, K., Del Rosso, G., . . . Petrucelli, L. (2020). C9orf72 poly(GR) aggregation induces TDP-43 proteinopathy. *Sci Transl Med, 12*(559). doi:10.1126/scitranslmed.abb3774

Coyne, A. N., Yamada, S. B., Siddegowda, B. B., Estes, P. S., Zaepfel, B. L., Johannesmeyer, J. S., . . . Zarnescu, D. C. (2015). Fragile X protein mitigates TDP-43 toxicity by remodeling RNA granules and restoring translation. *Hum. Mol. Genet, 24*(24), 6886-6898. doi:ddv389 [pii];10.1093/hmg/ddv389 [doi]

Coyne, A. N., Zaepfel, B. L., Hayes, L., Fitchman, B., Salzberg, Y., Luo, E. C., . . . Rothstein, J. D. (2020). G4C2 Repeat RNA Initiates a POM121-Mediated Reduction in Specific Nucleoporins in C9orf72 ALS/FTD. *Neuron, 107*(6), 1124-1140 e1111. doi:10.1016/j.neuron.2020.06.027

593 Cross, B. C., Bond, P. J., Sadowski, P. G., Jha, B. K., Zak, J., Goodman, J. M., . . . Harding, H. P. (2012). The
594 molecular basis for selective inhibition of unconventional mRNA splicing by an IRE1-binding small
595 molecule. *Proc Natl Acad Sci U S A, 109*(15), E869-878. doi:10.1073/pnas.1115623109
596 Cunningham, K. M., Maulding, K., Ruan, K., Senturk, M., Grima, J. C., Sung, H., . . . Lloyd, T. E. (2020).
597 TFEB/Mitf links impaired nuclear import to autophagolysosomal dysfunction in C9-ALS. *Elife, 9*.
598 doi:10.7554/eLife.59419
599 Dafinca, R., Scaber, J., Ababneh, N., Lalic, T., Weir, G., Christian, H., . . . Talbot, K. (2016). C9orf72
600 Hexanucleotide Expansions Are Associated with Altered Endoplasmic Reticulum Calcium
601 Homeostasis and Stress Granule Formation in Induced Pluripotent Stem Cell-Derived Neurons
602 from Patients with Amyotrophic Lateral Sclerosis and Frontotemporal Dementia. *Stem Cells, 34*(8),
603 2063-2078. doi:10.1002/stem.2388 [doi]
604 Daigle, J. G., Lanson, N. A., Jr., Smith, R. B., Casci, I., Maltare, A., Monaghan, J., . . . Pandey, U. B. (2013).
605 RNA-binding ability of FUS regulates neurodegeneration, cytoplasmic mislocalization and
606 incorporation into stress granules associated with FUS carrying ALS-linked mutations. *Hum. Mol.*
607 *Genet, 22*(6), 1193-1205. doi:dds526 [pii];10.1093/hmg/dds526 [doi]
608 DeJesus-Hernandez, M., Mackenzie, I. R., Boeve, B. F., Boxer, A. L., Baker, M., Rutherford, N. J., . . .
609 Rademakers, R. (2011). Expanded GGGGCC hexanucleotide repeat in noncoding region of
610 C9ORF72 causes chromosome 9p-linked FTD and ALS. *Neuron, 72*(2), 245-256. doi:S0896-
611 6273(11)00828-2 [pii];10.1016/j.neuron.2011.09.011 [doi]
612 Deniz, A. A. (2020). Networking and Dynamic Switches in Biological Condensates. *Cell, 181*(2), 228-230.
613 doi:10.1016/j.cell.2020.03.056
614 Donnelly, C. J., Zhang, P. W., Pham, J. T., Haeusler, A. R., Mistry, N. A., Vidensky, S., . . . Rothstein, J. D.
615 (2013). RNA toxicity from the ALS/FTD C9ORF72 expansion is mitigated by antisense intervention.
616 *Neuron, 80*(2), 415-428. doi:S0896-6273(13)00918-5 [pii];10.1016/j.neuron.2013.10.015 [doi]
617 Figley, M. D., Bieri, G., Kolaitis, R. M., Taylor, J. P., & Gitler, A. D. (2014). Profilin 1 associates with stress
618 granules and ALS-linked mutations alter stress granule dynamics. *J. Neurosci, 34*(24), 8083-8097.
619 doi:34/24/8083 [pii];10.1523/JNEUROSCI.0543-14.2014 [doi]
620 Gendron, T. F., Bieniek, K. F., Zhang, Y. J., Jansen-West, K., Ash, P. E., Caulfield, T., . . . Petrucelli, L. (2013).
621 Antisense transcripts of the expanded C9ORF72 hexanucleotide repeat form nuclear RNA foci and
622 undergo repeat-associated non-ATG translation in c9FTD/ALS. *Acta Neuropathol, 126*(6), 829-844.
623 doi:10.1007/s00401-013-1192-8 [doi]
624 Gilks, N., Kedersha, N., Ayodele, M., Shen, L., Stoecklin, G., Dember, L. M., & Anderson, P. (2004). Stress
625 granule assembly is mediated by prion-like aggregation of TIA-1. *Mol. Biol. Cell, 15*(12), 5383-
626 5398. doi:10.1091/mbc.E04-08-0715 [doi];E04-08-0715 [pii]
627 Guillen-Boixet, J., Kopach, A., Holehouse, A. S., Wittmann, S., Jahnel, M., Schlussler, R., . . . Franzmann, T.
628 M. (2020). RNA-Induced Conformational Switching and Clustering of G3BP Drive Stress Granule
629 Assembly by Condensation. *Cell, 181*(2), 346-361 e317. doi:10.1016/j.cell.2020.03.049
630 Haeusler, A. R., Donnelly, C. J., Periz, G., Simko, E. A., Shaw, P. G., Kim, M. S., . . . Wang, J. (2014). C9orf72
631 nucleotide repeat structures initiate molecular cascades of disease. *Nature, 507*(7491), 195-200.
632 doi:nature13124 [pii];10.1038/nature13124 [doi]
633 Jain, S., Wheeler, J. R., Walters, R. W., Agrawal, A., Barsic, A., & Parker, R. (2016). ATPase-Modulated Stress
634 Granules Contain a Diverse Proteome and Substructure. *Cell, 164*(3), 487-498. doi:S0092-
635 8674(15)01702-X [pii];10.1016/j.cell.2015.12.038 [doi]
636 Kedersha, N., Panas, M. D., Achorn, C. A., Lyons, S., Tisdale, S., Hickman, T., . . . Anderson, P. (2016). G3BP-
637 Caprin1-USP10 complexes mediate stress granule condensation and associate with 40S subunits.
638 *J. Cell Biol, 212*(7), 845-860. doi:jcb.201508028 [pii];10.1083/jcb.201508028 [doi]

639 Kedersha, N., Tisdale, S., Hickman, T., & Anderson, P. (2008). Real-time and quantitative imaging of
640 mammalian stress granules and processing bodies. *Methods Enzymol, 448*, 521-552. doi:S0076-
641 6879(08)02626-8 [pii];10.1016/S0076-6879(08)02626-8 [doi]
642 Kim, E. K., & Choi, E. J. (2010). Pathological roles of MAPK signaling pathways in human diseases. *Biochim*
643 *Biophys Acta, 1802*(4), 396-405. doi:10.1016/j.bbadis.2009.12.009
644 Kwon, I., Xiang, S., Kato, M., Wu, L., Theodoropoulos, P., Wang, T., . . . McKnight, S. L. (2014). Poly-
645 dipeptides encoded by the C9orf72 repeats bind nucleoli, impede RNA biogenesis, and kill cells.
646 *Science, 345*(6201), 1139-1145. doi:science.1254917 [pii];10.1126/science.1254917 [doi]
647 Lee, K. H., Zhang, P., Kim, H. J., Mitrea, D. M., Sarkar, M., Freibaum, B. D., . . . Taylor, J. P. (2016). C9orf72
648 Dipeptide Repeats Impair the Assembly, Dynamics, and Function of Membrane-Less Organelles.
649 *Cell, 167*(3), 774-788. doi:S0092-8674(16)31383-6 [pii];10.1016/j.cell.2016.10.002 [doi]
650 Lee, S., Shang, Y., Redmond, S. A., Urisman, A., Tang, A. A., Li, K. H., . . . Huang, E. J. (2016). Activation of
651 HIPK2 Promotes ER Stress-Mediated Neurodegeneration in Amyotrophic Lateral Sclerosis.
652 *Neuron, 91*(1), 41-55. doi:10.1016/j.neuron.2016.05.021
653 Li, Y. R., King, O. D., Shorter, J., & Gitler, A. D. (2013). Stress granules as crucibles of ALS pathogenesis. *J.*
654 *Cell Biol, 201*(3), 361-372. doi:jcb.201302044 [pii];10.1083/jcb.201302044 [doi]
655 Lin, Y., Mori, E., Kato, M., Xiang, S., Wu, L., Kwon, I., & McKnight, S. L. (2016). Toxic PR Poly-Dipeptides
656 Encoded by the C9orf72 Repeat Expansion Target LC Domain Polymers. *Cell, 167*(3), 789-802 e712.
657 doi:10.1016/j.cell.2016.10.003
658 Lin, Y., Protter, D. S., Rosen, M. K., & Parker, R. (2015). Formation and Maturation of Phase-Separated
659 Liquid Droplets by RNA-Binding Proteins. *Mol. Cell, 60*(2), 208-219. doi:S1097-2765(15)00664-4
660 [pii];10.1016/j.molcel.2015.08.018 [doi]
661 Ling, S. C., Polymenidou, M., & Cleveland, D. W. (2013). Converging mechanisms in ALS and FTD: disrupted
662 RNA and protein homeostasis. *Neuron, 79*(3), 416-438. doi:S0896-6273(13)00657-0
663 [pii];10.1016/j.neuron.2013.07.033 [doi]
664 Liu, F. L., Morderer, D., Wren, M. C., Vettleson-Trutza, S. A., Wang, Y. Z., Rabichow, B. E., . . . Rossoll, W.
665 (2022). Proximity proteomics of C9orf72 dipeptide repeat proteins identifies molecular
666 chaperones as modifiers of poly-GA aggregation. *Acta Neuropathologica Communications, 10*(1).
667 doi:ARTN 22

668 10.1186/s40478-022-01322-x
669 Liu, L., Zhang, K., Sandoval, H., Yamamoto, S., Jaiswal, M., Sanz, E., . . . Bellen, H. J. (2015). Glial lipid
670 droplets and ROS induced by mitochondrial defects promote neurodegeneration. *Cell, 160*(1-2),
671 177-190. doi:S0092-8674(14)01589-X [pii];10.1016/j.cell.2014.12.019 [doi]
672 Martin-Blanco, E., Gampel, A., Ring, J., Virdee, K., Kirov, N., Tolkovsky, A. M., & Martinez-Arias, A. (1998).
673 puckered encodes a phosphatase that mediates a feedback loop regulating JNK activity during
674 dorsal closure in Drosophila. *Genes & Development, 12*(4), 557-570. doi:DOI
675 10.1101/gad.12.4.557
676 Mizielinska, S., Gronke, S., Niccoli, T., Ridler, C. E., Clayton, E. L., Devoy, A., . . . Isaacs, A. M. (2014). C9orf72
677 repeat expansions cause neurodegeneration in Drosophila through arginine-rich proteins.
678 *Science, 345*(6201), 1192-1194. doi:science.1256800 [pii];10.1126/science.1256800 [doi]
679 Mori, K., Arzberger, T., Grasser, F. A., Gijselinck, I., May, S., Rentzsch, K., . . . Edbauer, D. (2013).
680 Bidirectional transcripts of the expanded C9orf72 hexanucleotide repeat are translated into
681 aggregating dipeptide repeat proteins. *Acta Neuropathol, 126*(6), 881-893. doi:10.1007/s00401-
682 013-1189-3 [doi]
683 Mori, K., Weng, S. M., Arzberger, T., May, S., Rentzsch, K., Kremmer, E., . . . Edbauer, D. (2013). The C9orf72
684 GGGGCC repeat is translated into aggregating dipeptide-repeat proteins in FTLD/ALS. *Science,*
685 *339*(6125), 1335-1338. doi:science.1232927 [pii];10.1126/science.1232927 [doi]

686 Ohn, T., Kedersha, N., Hickman, T., Tisdale, S., & Anderson, P. (2008). A functional RNAi screen links O-
687 GlcNAc modification of ribosomal proteins to stress granule and processing body assembly. *Nat.*
688 *Cell Biol, 10*(10), 1224-1231. doi:ncb1783 [pii];10.1038/ncb1783 [doi]
689 Protter, D. S., & Parker, R. (2016). Principles and Properties of Stress Granules. *Trends Cell Biol, 26*(9), 668-
690 679. doi:S0962-8924(16)30047-2 [pii];10.1016/j.tcb.2016.05.004 [doi]
691 Renton, A. E., Majounie, E., Waite, A., Simon-Sanchez, J., Rollinson, S., Gibbs, J. R., . . . Traynor, B. J. (2011).
692 A hexanucleotide repeat expansion in C9ORF72 is the cause of chromosome 9p21-linked ALS-FTD.
693 *Neuron, 72*(2), 257-268. doi:S0896-6273(11)00797-5 [pii];10.1016/j.neuron.2011.09.010 [doi]
694 Ring, J. M., & Arias, A. M. (1993). Puckered, a Gene Involved in Position-Specific Cell-Differentiation in the
695 Dorsal Epidermis of the Drosophila Larva. *Development*, 251-259. Retrieved from <Go to
696 ISI>://WOS:A1993NP85500027
697 Ritson, G. P., Custer, S. K., Freibaum, B. D., Guinto, J. B., Geffel, D., Moore, J., . . . Taylor, J. P. (2010). TDP-
698 43 mediates degeneration in a novel Drosophila model of disease caused by mutations in
699 VCP/p97. *J. Neurosci, 30*(22), 7729-7739. doi:30/22/7729 [pii];10.1523/JNEUROSCI.5894-09.2010
700 [doi]
701 Ritson, G. P., Custer, S. K., Freibaum, B. D., Guinto, J. B., Geffel, D., Moore, J., . . . Taylor, J. P. (2010). TDP-
702 43 mediates degeneration in a novel Drosophila model of disease caused by mutations in
703 VCP/p97. *J Neurosci, 30*(22), 7729-7739. doi:10.1523/JNEUROSCI.5894-09.2010
704 Rossetto, D., Avvakumov, N., & Cote, J. (2012). Histone phosphorylation: a chromatin modification
705 involved in diverse nuclear events. *Epigenetics, 7*(10), 1098-1108. doi:10.4161/epi.21975
706 Sahana, T. G., & Zhang, K. (2021). Mitogen-Activated Protein Kinase Pathway in Amyotrophic Lateral
707 Sclerosis. *Biomedicines, 9*(8). doi:10.3390/biomedicines9080969
708 Sakae, N., Bieniek, K. F., Zhang, Y. J., Ross, K., Gendron, T. F., Murray, M. E., . . . Dickson, D. W. (2018). Poly-
709 GR dipeptide repeat polymers correlate with neurodegeneration and Clinicopathological subtypes
710 in C9ORF72-related brain disease. *Acta Neuropathol Commun, 6*(1), 63. doi:10.1186/s40478-018-
711 0564-7
712 Sanders, D. W., Kedersha, N., Lee, D. S. W., Strom, A. R., Drake, V., Riback, J. A., . . . Brangwynne, C. P.
713 (2020). Competing Protein-RNA Interaction Networks Control Multiphase Intracellular
714 Organization. *Cell, 181*(2), 306-324 e328. doi:10.1016/j.cell.2020.03.050
715 Shi, Y., Lin, S., Staats, K. A., Li, Y., Chang, W. H., Hung, S. T., . . . Ichida, J. K. (2018). Haploinsufficiency leads
716 to neurodegeneration in C9ORF72 ALS/FTD human induced motor neurons. *Nat Med, 24*(3), 313-
717 325. doi:10.1038/nm.4490
718 Sone, M., Zeng, X., Larese, J., & Ryoo, H. D. (2013). A modified UPR stress sensing system reveals a novel
719 tissue distribution of IRE1/XBP1 activity during normal Drosophila development. *Cell Stress*
720 *Chaperones, 18*(3), 307-319. doi:10.1007/s12192-012-0383-x
721 Stricker, S. H., Koferle, A., & Beck, S. (2017). From profiles to function in epigenomics. *Nat Rev Genet,*
722 *18*(1), 51-66. doi:10.1038/nrg.2016.138
723 Tiwari, V. K., Stadler, M. B., Wirbelauer, C., Paro, R., Schubeler, D., & Beisel, C. (2011). A chromatin-
724 modifying function of JNK during stem cell differentiation. *Nat Genet, 44*(1), 94-100.
725 doi:10.1038/ng.1036
726 Urano, F., Wang, X., Bertolotti, A., Zhang, Y., Chung, P., Harding, H. P., & Ron, D. (2000). Coupling of stress
727 in the ER to activation of JNK protein kinases by transmembrane protein kinase IRE1. *Science,*
728 *287*(5453), 664-666. doi:10.1126/science.287.5453.664
729 Wheeler, J. R., Matheny, T., Jain, S., Abrisch, R., & Parker, R. (2016). Distinct stages in stress granule
730 assembly and disassembly. *Elife, 5*. doi:10.7554/eLife.18413
731 Xu, Z., Poidevin, M., Li, X., Li, Y., Shu, L., Nelson, D. L., . . . Jin, P. (2013). Expanded GGGGCC repeat RNA
732 associated with amyotrophic lateral sclerosis and frontotemporal dementia causes

neurodegeneration. *Proc. Natl. Acad. Sci. U. S. A, 110*(19), 7778-7783. doi:1219643110 [pii];10.1073/pnas.1219643110 [doi]

Yang, J., Wu, Z., Renier, N., Simon, D. J., Uryu, K., Park, D. S., . . . Tessier-Lavigne, M. (2015). Pathological axonal death through a MAPK cascade that triggers a local energy deficit. *Cell, 160*(1-2), 161-176. doi:10.1016/j.cell.2014.11.053

Yang, P., Mathieu, C., Kolaitis, R. M., Zhang, P., Messing, J., Yurtsever, U., . . . Taylor, J. P. (2020). G3BP1 Is a Tunable Switch that Triggers Phase Separation to Assemble Stress Granules. *Cell, 181*(2), 325-345 e328. doi:10.1016/j.cell.2020.03.046

Zhang, K., Daigle, J. G., Cunningham, K. M., Coyne, A. N., Ruan, K., Grima, J. C., . . . Lloyd, T. E. (2018). Stress Granule Assembly Disrupts Nucleocytoplasmic Transport. *Cell, 173*(4), 958-971 e917. doi:10.1016/j.cell.2018.03.025

Zhang, K., Donnelly, C. J., Haeusler, A. R., Grima, J. C., Machamer, J. B., Steinwald, P., . . . Rothstein, J. D. (2015). The C9orf72 repeat expansion disrupts nucleocytoplasmic transport. *Nature, 525*(7567), 56-61. doi:nature14973 [pii];10.1038/nature14973 [doi]

Zhang, Q., Bhattacharya, S., Pi, J., Clewell, R. A., Carmichael, P. L., & Andersen, M. E. (2015). Adaptive Posttranslational Control in Cellular Stress Response Pathways and Its Relationship to Toxicity Testing and Safety Assessment. *Toxicol Sci, 147*(2), 302-316. doi:10.1093/toxsci/kfv130

Zhang, Y. J., Gendron, T. F., Ebbert, M. T. W., O'Raw, A. D., Yue, M., Jansen-West, K., . . . Petrucelli, L. (2018). Poly(GR) impairs protein translation and stress granule dynamics in C9orf72-associated frontotemporal dementia and amyotrophic lateral sclerosis. *Nat Med, 24*(8), 1136-1142. doi:10.1038/s41591-018-0071-1

Zhang, Y. J., Guo, L., Gonzales, P. K., Gendron, T. F., Wu, Y., Jansen-West, K., . . . Petrucelli, L. (2019). Heterochromatin anomalies and double-stranded RNA accumulation underlie C9orf72 poly(PR) toxicity. *Science, 363*(6428). doi:10.1126/science.aav2606

Zu, T., Liu, Y., Banez-Coronel, M., Reid, T., Pletnikova, O., Lewis, J., . . . Ranum, L. P. (2013). RAN proteins and RNA foci from antisense transcripts in C9ORF72 ALS and frontotemporal dementia. *Proc. Natl. Acad. Sci. U. S. A, 110*(51), E4968-E4977. doi:1315438110 [pii];10.1073/pnas.1315438110 [doi]